Track-based aerodynamic testing of a two-truck platoon

McAuliffe, Brian; Smith, Patrick; Raeesi, Arash; Hoffman, Mark; Bevly, David M.

Publisher's version / Version de l'éditeur:
https://doi.org/10.4271/2021-01-0941
SAE International Journal of Advances and Current Practices in Mobility, SAE Technical Paper Series, 1, 2021-04-06

2021-01-0941 Published 06 Apr 2021

Track-Based Aerodynamic Testing of a Two-Truck Platoon

Brian McAuliffe National Research Council Canada

Patrick Smith Auburn University

Arash Raeesi National Research Council Canada

Mark Hoffman and David M. Bevly Auburn University

Citation: McAuliffe, B., Smith, P., Raeesi, A., Hoffman, M. et al., "Track-Based Aerodynamic Testing of a Two-Truck Platoon," *SAE Int. J. Advances & Curr. Prac. in Mobility* 3(3):1450-1472, 2021, doi:10.4271/2021-01-0941.

This article was presented at the WCX World Congress Experience Digital Summit, April 13-15, 2021.

Abstract

Fuel savings from truck platooning are generally attributed to an aerodynamic drag-reduction phenomena associated with close-proximity driving. The current paper is the third in a series of papers documenting track testing of a two-truck platoon with a Cooperative Adaptive Cruise Control (CACC) system where fuel savings and aerodynamics measurements were performed simultaneously. Constant-speed road-load measurements from instrumented driveshafts and on-board wind anemometry were combined with vehicle measurements to calculate the aerodynamic drag-area of the vehicles.

The drag-area results are presented for each vehicle in the two-truck platoon, and the corresponding drag-area reductions are shown for a variety of conditions: gap separation distances (9 m to 87 m), lateral offsets (up to 1.3 m), dry-van and flatbed trailers, and in the presence of surrounding traffic. For the standard aligned platoon, the results demonstrate up to 8% drag reduction for the lead vehicle, with drag reductions exceeding 20% for the trailing vehicle at some yaw angles. Wind-velocity measurements on the following truck suggest that the drag-area reductions are due to a combined effect of reduced apparent wind speed and reduced effective yaw angle in the wake of the lead truck. In the presence of a three-vehicle traffic pattern forward of a single truck, drag-area reductions on the order of 10% were observed relative to the same truck travelling in isolation. When platooning with this surrounding-traffic pattern, the trends and magnitudes of aerodynamic drag reduction are shown to be retained, relative to the platoon in the absence of other traffic, corroborating observed trends in of fuel-savings performed simultaneously.

As a supplement to the current study, a first-of-its-kind coast-down test was undertaken with the two-truck platoon where the CACC system was used to maintain a constant distance between the vehicles during each coast. The CACC system was used on the following vehicle when the lead vehicle was coasting and on the lead vehicle when the follower was coasting. Despite some scatter in the data from this proof-of-concept study, the results are consistent with those of the principal constant-speed measurement technique of this paper. This preliminary study demonstrates that the coast-down test method, which previously was only applied for single vehicles, is also applicable to vehicle platoons.

Introduction

The aerodynamic benefits of bodies in close proximity is being exploited by emerging truck-platooning technologies. At close longitudinal distance, following trucks benefit from being immersed in the wake of the leading vehicles, with some studies suggesting this effect persists to distances in excess of 100 m [1, 2, 3]. At distances below about 15 meters, a leading vehicle can benefit from the high-pressure in the airflow forward of the trailing trucks, increasing the lead truck's base pressure and reducing the overall pressure drag on the vehicle [4, 5]. For truck platoons of three or more vehicles, the middle vehicles can benefit from both front and rear aerodynamic effects [1, 6, 7]. To date, the aerodynamic drag reduction associated with truck platooning of modern North-American trucks has been quantified by means of wind tunnel testing [7, 8] or computational fluid dynamics (CFD) simulations [4, 5, 6, 9, 10, 11]. McAuliffe & Ahmadi-Baloutaki [8] demonstrated drag reductions on the order of 20% for the lead and trailing vehicles at distances below about 1 vehicle length. Ortega & Salari [7] demonstrated similar drag reductions for two-truck platoons over the same range of separation distances, but also highlighted the drag reductions for three-truck platoons and the benefits at larger vehicle separation distances (order of 5% wind-averaged drag reduction at 73 m

full-scale separations). Both of these wind-tunnel studies, undertaken with aerodynamic sleeper-cab tractors and box-van trailers, also examined the influence of different trailer configurations and the effects of lateral misalignment of two truck platoons, both effects of which showed measurable changes in the drag-reduction performance of truck platooning. The CFD studies noted above have also shown similar trends and magnitudes as the wind tunnel studies.

Track testing to quantify the aerodynamic performance of heavy-duty vehicles is becoming common practice for greenhouse-gas (GHG) regulations in North America and Europe [12, 13]. In North America, the Greenhouse-gas Emissions Model (GEM) is used for regulatory reporting and requires an aerodynamic input based on the measured drag area (C_DA) referenced to a standard coast-down test method. In Europe, however, the Vehicle Energy Consumption Calculation TOol (VECTO) requires a C_DA referenced to a standard constant-speed test approach. Both the coast-down and constant-speed methods are based on a balance of forces on the vehicle in the direction of motion, with the former gauging the road load from the vehicle deceleration and the latter using the tractive force required to keep the vehicle at speed [14, 15]. Delgado et al. [15] discuss the two methods, as defined by the respective North American and European regulations, and describe the relative merits and deficiencies of each. The constant-speed method generally requires greater cost in the instrumentation for testing to measure the vehicle road load as accurately as possible, while relying on models to convert the data to a reference zero-yaw-angle drag-area value. The coast-down method, on the other hand, generally requires less critical instrumentation for testing but requires greater cost in component performance tests to account for speed-dependent mechanical resistances and supplemental evaluations to convert the data to a reference 4.5° -yaw-angle drag-area value.

On-road assessments of the aerodynamic benefits of truck platooning have, to date, been based on fuel-economy measurements from which the aerodynamic benefits are inferred but not quantified directly [1, 9, 16, 17, 18, 19, 20, 21, 22, 23, 24]. This paper documents two studies, using the same truck-platooning system, for which each has used one of the two above-noted aerodynamic track-test methods to measure the drag-area reduction (ΔC_DA) of a two-truck platoon. In parallel with a detailed fuel-economy study, the constant-speed method was used to quantify the aerodynamic drag of the two trucks in the platoon simultaneously for a range of separation distances, with and without lateral offsets, and in the presence of surrounding traffic. The basis for this study was a demonstration of the viability of the constant-speed-aerodynamic measurement technique for a three-truck platoon presented by McAuliffe [25], recommendations from which have guided the current study. Additionally, a proof-of-concept coast-down study has been undertaken and is presented here with the same tractors and platooning system, for two separation distances, using a novel application of the platooning system to maintain a fixed separation of the vehicles while coasting.

A secondary purpose of this study is to verify that aerodynamic drag reduction is the dominant source of fuel savings associated with truck platooning. The fuel-saving behavior of the two-truck platoon from the concurrent fuel economy study is shown in Figures 1 and 2 (reproduced from [2, 3]). Consistent with other fuel-consumption tests of truck platoons, these results demonstrate lead-truck fuel savings at smaller separation distances, with

FIGURE 1 Fuel-consumption results for the two-truck platoon in aligned and offset configurations, measured on straight track segments only (reproduced with permission from [2]).

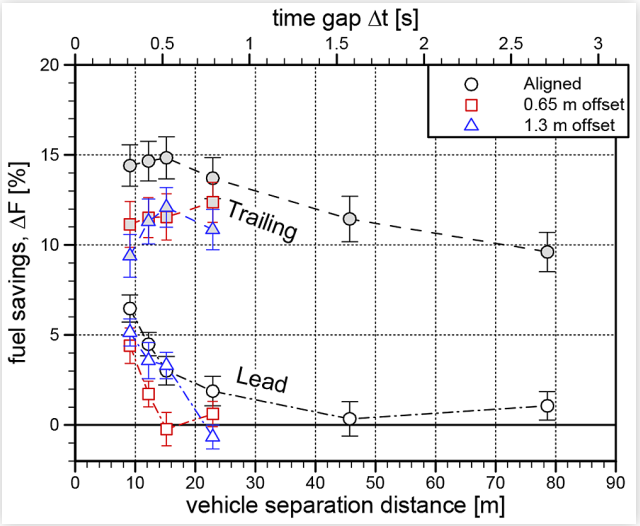

FIGURE 2 Fuel-consumption results for the two-truck platoon with and without surrounding traffic (reproduced with permission from [3]).

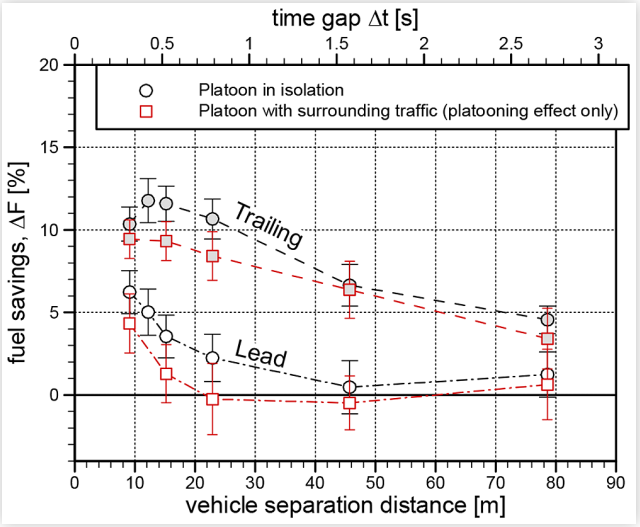

trailing-truck fuel savings persisting to large distances, whether in traffic or in isolation. When controlled lateral offsets or surrounding traffic was introduced on the track, the fuel savings were marginally decreased for each which indicates that the standard, isolated and aligned truck platooning investigations produce a maximum in the potential drag-reduction benefits from this technology. The purpose of the current study is to quantify the aerodynamic performance of this two-truck platoon under the variety of conditions examined on the track to provide data from which aerodynamic-performance models can be developed, and to provide real-world validation data for wind-tunnel and CFD approaches.

Test Setup and Procedures

CACC System Description

A cooperative adaptive cruise control (CACC) platooning system is used in the current test campaign. The system allows for automated longitudinal control of a following vehicle, while the lead vehicle operates using stock adaptive cruise control (ACC). The CACC system was previously documented [2, 26, 27], but a few items are provided here for clarity. Overall, the system has three components: a dedicated short-range communication (DSRC) radio network for vehicle-to-vehicle (V2V) communication, the upper-level control system, and the by-wire kit. The upper-level system includes the software and algorithms necessary for CACC platooning. The by-wire kit is the vehicle interface where data are read from the CAN bus. Additionally, automated vehicle control is accomplished by generating controller-area-network (CAN) commands and controlling the vehicle through the by-wire kit.

The system is implemented for two heavy-duty trucks and enables CACC platooning. On the lead vehicle, the same CACC system exists even though control is accomplished by the stock ACC. The system collects and processes sensor data and then transmits them across the V2V network for the following vehicle to use. In the current work, a variety of mixed-traffic scenarios are introduced. These scenarios include tests where the "CACC controlled" second vehicle follows another vehicle, i.e. a passenger vehicle. This is accomplished by placing an external, mobile system that mimics the CACC system setup. The external system includes a GPS receiver, DSRC radio, and computer. Functionally, this system allows for the heavy-duty truck to "platoon" with any vehicle in which the mobile system is placed.

For longitudinal control, the CACC system objective is to follow the lead vehicle at the specified reference distance. In this testing, the fuel-savings results are quantified as a function of following distance. As documented in the first paper of this series [2], it is important to consider the control system performance when evaluating the platoon results, which was shown to have a gap error average and deviation of 0.00 and 0.34 m over an entire test.

Test Vehicles

Two aerodynamically-treated Class 8 heavy-duty tractors with 53 ft dry-van trailers were used as test vehicles in the fuel-economy study, shown in Figures 3 and 4. Both lead and follower tractors were Peterbilt 579's (model year 2015), but each had a different engine (Paccar MX-13 for the lead and Cummins ISX15 for the follower). The identical Manac trailers were outfitted with Transtex EDGE Skirts (2330 model) and Stemco Trailer Tails (Trident model) with the fifth wheel and bogie in the California positions (45 inch tractor-trailer gap and rear axle 10 ft from trailer base). A Manac 53-ft flat-bed trailer was also used for a small subset of tests (see Figure 5). More about the test vehicle are found in [2, 3]. The frontal area of each truck, estimated as trailer width×trailer height, is 10.7 m^2 for the dry-van-trailer configurations and only slightly less with the flat-bed trailer due to the large tractor roof fairing. The SAE J1321 fuel-consumption test procedure [28] requires identical vehicles to be used. In this study, however, the test vehicles differed from each other (different engines) and from the control vehicle (different make and model) and therefore this test program does not strictly conform to the SAE J1321 requirements. All tractors are aerodynamically-treated with high roof fairings, chassis skirts, side extenders, and aerodynamic bumpers, and were therefore expected to react similarly to changes in the environment that affect aerodynamic performance, particularly the ambient winds.

The simultaneous fuel-economy tests required representative cargo weights in the trailers, which were ballasted to provide a total vehicle mass of 29,500 kg (65,000 lb). The trailers were ballasted using concrete blocks aligned evenly along the centerline of the trailer. Fuel levels in the main tanks

FIGURE 3 Side-view photograph of Trucks 1 and 2 with 53-ft dry-van trailer and 9 m (30 ft) spacing.

FIGURE 4 Offset front-view photograph of Trucks 1 and 2 with 53-ft dry-van trailer and 9 m (30 ft) spacing.

FIGURE 5 Side-view photograph of Truck 1 with the 53-ft flatbed trailer and Truck 2 with the 53-ft dry-van trailer at 9 m (30 ft) spacing.

of the trucks were adjusted to match the weight amongst all three vehicles. The flat-bed trailer was also ballasted using concrete blocks clustered near the middle of the bed.

To examine the impact of surrounding traffic, additional vehicles were introduced onto the track in a controlled manner. These vehicles were passive, in that they were introduced to modify the boundary conditions for the test and no measurements were acquired from them. Up to seven additional light-duty passenger vehicles were used: 1 compact SUV, 3 mid-sized SUVs, 1 compact sedan, 1 mid-size pickup truck, and 1 full-size pickup truck. Three of these vehicles (1 mid-size SUV, 1 compact sedan, and 1 full-size pickup truck) were used for a large portion of the testing to provide an arrangement of vehicles upstream of the trucks that would be representative of driving in highway traffic conditions.

Test Site

Testing was performed at the Transport Canada Motor Vehicle Test Centre operated by PMG Technologies in Blainville, Quebec at 45.70 latitude and -73.87 longitude. The "Bravo" track was used for testing, which is a high-speed track with a primary surface of rain-grooved concrete. The track is 6.5-km (4.0-mile) long oval shape with two straight 1.6-km (1.0-mile) sections, and two 1.6-km (1.0-mile) constant-curvature banked sections. An aerial view of the test track is shown in Figure 6.

Data Acquisition

To understand the behaviour of the tested vehicles better, a variety of parameters on each truck were measured and recorded using an IMC data acquisition system. Data included geographical position, on-board wind measurements, cooling flow measurements, ambient and under-hood temperature measurements, engine-cooling performance, driveshaft torque measurements, in addition to several variables from the vehicle network using the CAN bus protocol. Geographical latitude and longitude of all trucks were recorded at a rate of 5 Hz using GPS antennas that were mounted on the roof of each tractor.

FIGURE 6 Aerial view of the test track; Location of Track-side anemometers and truck refuelling and staging are shown by yellow circles.

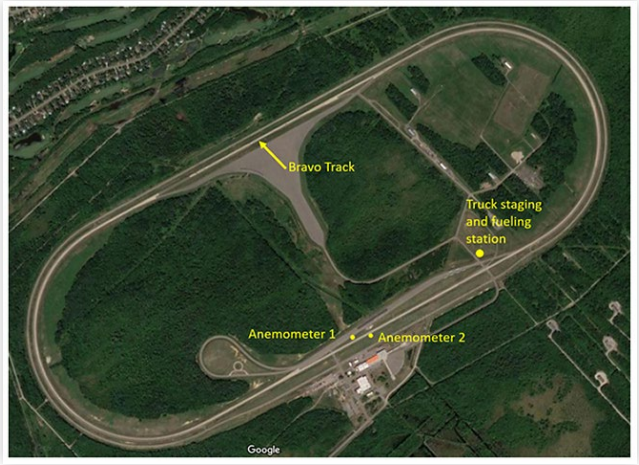

Maps Data: Google, © CNES / Airbus, Maxar Technologies.

Terrestrial Wind Measurements

Site and track-side wind measurements were performed during the test campaign. The on-site weather station, which is positioned at 3 m height and approximately 50 m from the track, provided the wind speed and direction, along with the temperature and barometric pressure. 10-second and 10-minute mean data were available from this weather station. To collect wind data closer to the track and at vehicle mid-height, two ultrasonic anemometers were placed adjacent to the south-side straight segment of the track (locations shown in Figure 6), approximately 8 m from either side of the track centreline, with the sensor 2 m above the track surface. These track-side ultrasonic anemometers were used as the primary reference to calibrate on-board wind instruments. Data were acquired from the track-side anemometers at a rate of 20 Hz.

On-Board Wind Measurements

On-board wind measurements were performed for Trucks 1 and 2 using "Cobra Probes" located at the front of the tractor on a tripod boom. Truck 1 was also equipped with an additional Cobra Probe mounted above the trailer at approximately 5 m above the ground. The Cobra Probe, manufactured by Turbulent Flow Instrumentation Pty Ltd., is a fast-response four-hole pressure probe that measures the fluctuations in wind speed, wind direction, and pressure [29]. The locations of the Cobra Probes on Truck 1 are shown in Figure 7. The Cobra Probe data were acquired at a sampling rate of 100 Hz. Due to the proximity of the Cobra Probes to the vehicle, their measurements do not represent the freestream wind conditions. The track-side-anemometer data

FIGURE 7 Location of grille vane anemometer (lower red circle), front Cobra Probe (middle red circle), and trailer Cobra Probe (top red circle) on Truck 1.

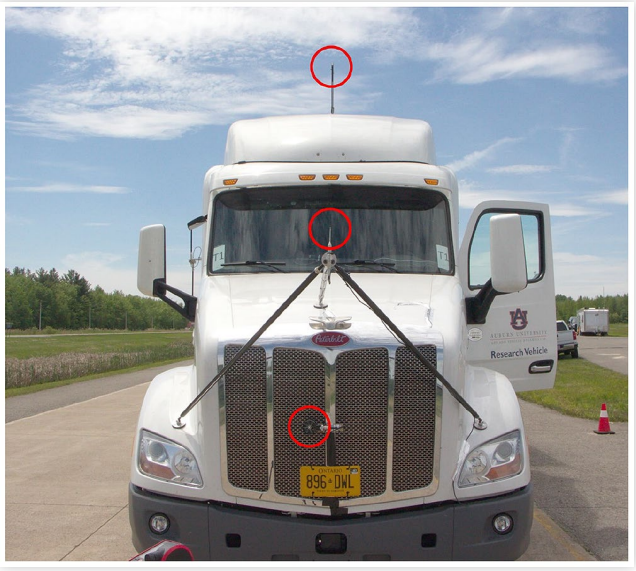

have been used to calibrate the on-board Cobra-probe data using the method of Tanguay [30]. This method estimates the location at which the winds advecting past the track-side anemometer intersect the trajectory of the truck-mounted cobra probe, and use the corresponding measurements (averaged over 0.5 seconds) to develop a calibration for the wind speed and yaw angle. A calibration data point is acquired once each test lap during the baseline test runs, with all isolated-platoon tests providing additional calibration points for Truck 1. The calibration differs slightly for each truck, but the forward mounted cobra probe measures approximately 0.85 of the freestream wind speed and approximately 1.4 times the freestream yaw angle. The high-mounted probe on Truck 1 measures approximately 105% of the freestream wind speed and approximately 1.4 times the freestream yaw angle.

Drive-Shaft Torque Measurements

To permit an analysis of the road load characteristics of the vehicles in platoon arrangement, the torque transferred through the drive shaft was measured. These measurements, when combined with the on-board wind measurements, permit an assessment of the aerodynamic drag forces acting on the vehicles. The torque measurements were performed using strain gauges on the drive shaft in a full-bridge arrangement and a wireless telemetry system (TECAT Performance Systems WISER 4000) to acquire the measurements. The data were acquired at a sampling rate 100 Hz.

Test Procedures

The high-speed test runs were performed simultaneously with fuel consumption measurements conducted according to the SAE J1321 Type II procedure [28]. To meet the minimum distance requirements of the J1321 procedure, each test run consisted of 13 laps providing 85 km (52 mi) of travel per run. A minimum of three test runs were performed for each high-speed condition, while single mid-speed and low-speed runs were performed for some test configurations. Only data acquired while travelling on the straight segments of the track were used for the analysis described herein.

Nine baseline runs were conducted throughout the test campaign, with the trucks spaced approximately 2 km apart from each other and from the control truck. For the isolated truck-platoon tests, the control truck was spaced between 2 km and 3 km from the truck platoon. The trucks remained in the right (outside) lane and maintained speed for the duration of the test runs using their respective cruise-control systems, with independent checks by a track-side radar located on the north-side straight segment of the track.

Tests with lateral offsets of 0.65 m and 1.3 m were performed, representing a quarter-truck width and a half-truck width, respectively. These offsets are shown in Figure 8. The lateral offsets were controlled manually by the driver but the "true" lateral offset was calculated as described by [2]. The lateral offset was maintained only on the straight segments of the track for which the standard deviation of the lateral position was evaluated to be on the order of 0.15 m for a typical run.

For the steady-state mixed-traffic tests, the lead truck followed a mid-size SUV at 78 m using the stock ACC system in the right (outside) lane, while in the left (inside) lane a full-size pickup truck and compact sedan were arranged longitudinally between the SUV and the truck as shown in Figures 9 and 10. This same "traffic" pattern was also used in the single-truck test and conducted independently for Truck 1 and Truck 2 to create "traffic baseline" performance for which to evaluate platoon effects on drag area while travelling with other traffic.

FIGURE 8 Photographs of quarter-truck-width offset (left) and half-truck-width offset (right) platoon arrangements.

FIGURE 9 Photograph of the side view of a truck platoon following the light-duty-vehicle traffic pattern.

FIGURE 10 Offset front-view photograph of the light-duty-vehicle traffic pattern in front of a single truck.

Constant-Speed Analysis

Equation of Motion

The concept of the constant-speed analysis is to infer the external forces acting on a vehicle based on the power required to maintain its speed. Figure 11 shows a simplified free-body diagram of a vehicle travelling at constant speed. The forces that affect forward motion to the vehicle are:

- Tractive Force (F_{Trac}) - Force delivered by the driven wheels to maintain speed.
- Aerodynamic Drag (F_{Aero}) - resistive force as the vehicle moves through the air;
- Rolling Resistance (F_{RR}) - resistive force due to deformation of the tire material at the interface with the ground;
- Grade Force (F_{Grade}) - component of the vehicle weight in the direction of motion due to the grade/inclination of the road surface from horizontal; and

The aerodynamic drag, rolling resistance, and grade force contribute to the Road Load (F_{RL}), which is the combination of external forces acting on the vehicle while in motion.

Applying Newton's 2nd law of motion in the direction of motion of the vehicle, the resulting equation is

$$m_e \frac{dV}{dt} = F_{Trac} - F_{Aero} - F_{RR} - F_{Grade} \tag{1}$$

for which m_e is the effective mass that includes the vehicle mass and the rotational inertia of the wheels and rotating drivetrain components. A typical value for the effective mass of each wheel of 56.7 kg (125 lb) has been used, based on measurements performed by the EPA for SmartWay verified tires with conventional steel-rims [14].

FIGURE 11 Free-body diagram of a vehicle at constant speed.

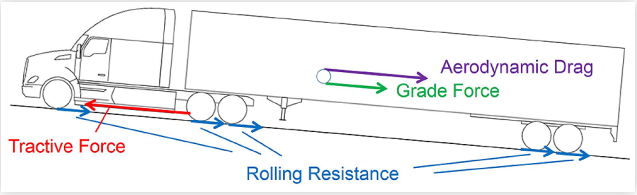

The constant-speed-analysis methods developed for the North-American and European GHG regulations [12, 13] assume that the vehicle is maintained at a constant speed at all times, and therefore, the vehicle's acceleration is zero and the inertial term on the left side of Equation 1 is set to zero. In practice, due to the significant weight of the vehicle combined with the non-level grade of the road surface and the inability of most cruise control systems to maintain a precise speed at all times, small speed changes can result in measurable inertial forces and this assumption may not be valid under all conditions. For example, with the current test program, changes in speed on the order of 0.5 km/h over a 10 second period were observed, which results in the inertial term of the equation of motion being on the order of 10% of the constant-speed road load. Therefore, the inertial term was included in the current analysis. This influence is exacerbated in the current study due to the cargo weight added to the trailer for the simultaneous fuel-consumption measurements.

The tractive force required to maintain the vehicle speed has been measured using a driveshaft torque meter (τ_{shaft}), installed on the drive-shaft between the transmission and the differential. Using the measurement of shaft rotational speed (ω_{shaft}), the tractive force delivered to the ground is

$$F_{Trac} = \frac{\tau_{shaft}\ \omega_{shaft}\ \eta}{V} \tag{2}$$

where V is the vehicle speed. The mechanical power loss between the driveshaft and the ground is introduced here through an efficiency factor (η) applied to the shaft power. Gururaja [31] measured the efficiency of several dual-drive-axle tractors, based on the relationship between driveshaft- and wheel-torque measurements, and found efficiency values in the range 91% to 94%. For the current analysis, a value of 92% has been assumed.

The aerodynamic drag force is the parameter of most interest for the current investigation. The drag force for a vehicle can be defined as

$$F_{Aero} = Q\ C_D(\psi, R_U)\ A \tag{3}$$

where the dynamic pressure of the wind (Q) is dependent on the air density (ρ) and wind speed relative to the vehicle (U):

$$Q = \frac{1}{2}\ \rho\ U^2 \tag{4}$$

In Equation 3, the drag coefficient (C_D) is shown as a function of two paremeters: yaw angle (ψ - wind angle relative to the vehicle) and wind-to-ground-speed ratio:

$$R_U = \frac{U}{V} \tag{5}$$

The wind-to-ground-speed ratio (R_U) has an influence on the drag coefficient due to the effect of ground and wheel motion. Based on wind-tunnel studies where these relative motions could be independently varied [32], these motions increase the drag experienced by the vehicle when compared to the stationary floor and wheel setup. This effect is due to a combination of changes to the flow patterns in the underbody and wheel wells and due to the windage drag associated with

the resistive aerodynamic torque on the spinning wheels. Therefore, the drag area of a vehicle is affected by this ratio. For example, the net drag area of a truck travelling at 80 km/h with a uniform 20 km/h headwind is not the same as that of the same truck travelling at 100 km/h with no winds. The lower wheel speed in the former case will result in a lower net drag area. When accounting for windage drag for the wheels, McAuliffe [32] showed a reduction in wind-averaged-drag coefficient of 0.037 when the wheel and ground motion were turned off in a wind tunnel study, which is approximately 8% of the 0° -yaw C_D of the test trucks in this study. Based on unpublished follow-on work by the first author, this change in C_D varies linearly with the wind-to-ground-speed ratio (R_U), with negligible influence of yaw angle. During the track testing, for which the SAE J1321 wind-speed limits were imposed (limit of 20 km/h), R_U may then vary from 0.8 to 1.2. Assuming the influence of wheel and ground speed observed by McAuliffe [32] applies to the trucks in this study, this would result in a 3% variation in drag coefficient depending on the strength of the winds. To account for this influence, the following correction to the drag-coefficient term has been included in the equation of motion:

$$C_D(\psi, R_U) = C_D(\psi) - \frac{\partial C_D}{\partial R_U}(R_U - 1) \tag{6}$$

where a value of 0.037 has been used for the $\partial C_D/\partial R_U$ term. For R_U greater than 1 (ground speed slower than effective wind speed) the measured drag coefficient will be lower than if the ground speed was the same as the wind speed, and this correction increases the drag coefficient accordingly. Conversely, for R_U smaller than 1, the correction increases the drag coefficient. Including this correction in the current analysis has improved the yaw symmetry of the results, indicating it is a justifiable correction. This may be one of the factors leading to the asymmetric $C_D(\psi)$ curves presented in Gururaja's constant-speed aerodynamic study [31].

The drag coefficient of heavy-duty vehicles has also been shown to have a dependence on Reynolds number and atmospheric turbulence. Recent data show that, for modern aerodynamic tractor-trailer combinations, the greatest influence of C_D to Reynolds number occurs for low speeds ($\lesssim$50 km/h) at which the drag force is smaller due to the low dynamic pressure [33, 34, 35]. As such, this Reynolds-number dependence is not expected to influence the results and has been neglected. With regards to turbulence, the elevated turbulence conditions under which the drag coefficient can be influenced are generally due to upstream traffic [36, 35]. In the current study, only the steady-mixed-traffic tests contain upstream traffic and the influence of those vehicles are quantified separately. Therefore, the turbulence influence on C_D is not modelled explicitly in Equation 3.

The results of this paper are presented using the drag area as the principal metric (C_DA), which precludes the requirement for an accurate measure of the vehicle frontal area in its calculation:

$$C_DA = \frac{F_{Aero}}{Q} \tag{7}$$

Drag area is useful for direct vehicle-to-vehicle comparisons when full-scale vehicles or models are used, as it represents the ratio of drag force to dynamic pressure without any requirement for geometric information.

The rolling resistance (F_{RR}) of a tire can be affected by many factors such as vertical load on the tire, inflation pressure, rotational speed, and ground texture. It is generally assumed that only vertical load influences the rolling resistance, and that all tires on the vehicle behave in the same manner such that a constant rolling-resistance coefficient (C_{RR}) for the vehicle can be assumed. This rolling resistance coefficient is defined as:

$$C_{RR} = \frac{F_{RR}}{F_z} \tag{8}$$

where F_z is the vertical load transferred through all wheels to the ground. For the low grade levels defined for most coast-down testing, this vertical load can be assumed equal to the vehicle weight ($F_z \approx W = mg$).

In recent years, it has come to light that the rolling resistance of heavy-duty-vehicle tires exhibit different characteristics in a coast-down environment than in a constant speed environment [14, 37]. In the current analysis, dependence of the rolling resistance to vehicle speed has also been included, along with a conventional temperature correction. As such, the rolling resistance term in Equation 1 is modelled as

$$F_{RR} = C_{RR}(V)W\left[1 + \frac{\partial C_{RR}}{\partial T}(T - 293)\right] \tag{9}$$

for which $\partial C_{RR}/\partial T$ is assumed to be 0.006 [38]. For the regulatory development studies performed in the mid 2010's, the EPA had several tire sets tested [37] over a range of constant-speed conditions. Applying the model of SAE J2452 [39] method, those data were modelled in the following form:

$$F_{RR} = P^{\alpha} L^{\beta} \left(a + bV + cV^2\right) \tag{10}$$

where P is the inflation pressure, L is the vertical load, V is the speed at the periphery of the tire, and α, β, a, b, and c are coefficients of the model. Using the results of the low-rolling-resistance tires tested, a model was developed by McAuliffe and Chuang [14] that defines the ratio of the rolling resistance coefficient to its near-zero-speed value (C_{RR0}), as follows:

$$R_{RR} = \frac{C_{RR}}{C_{RR0}} = 9.0\times10^{-8}V^4 + 1.0\times10^{-5}V^2 + 1.0 \tag{11}$$

where V is in m/s. Below 50 km/h (30 mph), there is no appreciable change in the rolling resistance coefficient, where as at 112 km/h (65 mph) the rolling-resistance coefficient is 9% higher than its low-speed value.

The grade force is calculated from the vehicle weight and the known grade of the track:

$$F_{Grade} = W\frac{dh}{ds} \tag{12}$$

The grade was defined based on post-processed GPS logs using real-time-kinetic (RTK) corrections [2], which provide centimetre-level accuracy of position.

Returning to the equation of motion (Equation 1), the force contributions can be grouped into those that are directly measurable and those that are inferred or calculated. The road load (F_{RL}), consisting of aerodynamic and rolling resistance

forces, represents the performance of the vehicle with respect to external loads, both of which are influenced by environmental factors. The road load is calculated from the measured tractive force, inertial loads and grade force, as follows:

$$F_{RL} = F_{Aero} + F_{RR} = F_{Trac} - m_e \frac{dV}{dt} - F_{Grade} \tag{13}$$

Based on the models defined above for the aerodynamic and rolling-resistance forces (Equations 3 through 11) and combined with the measured loads (Equations 2 and 12), Equation 13 can be solved to calculate $C_D(\psi)$ and C_{RR0}.

Solution Method

The manner in which Equation 13 is solved in this study for $C_D(\psi)A$ and C_{RR0} is similar to the constant-speed approach alternatively used by the North American GHG regulations [12].

The wind conditions along the track varied due to changes in the local vegetation environment and due to transient effects encountered at the start and end of each section of the track. Therefore, data were acquired over the middle 1.2 km of each straight segment of the track, and split into two 600 m data segments. At the test speed of 105 km/h, each of these segments represents approximately 20 seconds of data collection.

The road load for each 600 m-segment data point (index i) has been calculated as

$$F_{RLi} = \overline{\left[\frac{\tau_{shaft}\ \omega_{shaft}\ \eta}{V} - m_e \frac{dV}{dt} - W \frac{dh}{ds} \right]} \tag{14}$$

where the over-bar denotes an average over the segment duration. Most measurement signals have been low-pass filtered with a cut-off frequency of 0.2 Hz prior to calculating the segment-averaged road load values. For the vehicle-speed measurements, the random nature of the point-to-point uncertainty in the 5 Hz update-rate was found to be too noisy for calculating vehicle acceleration. The J1939-reported wheel speed parameters, sampled at 100 Hz from the vehicle CAN bus, were found to provide lower-noise signals but with bias offsets. The offsets of these wheel-speed measurements were quantified based on the 600 m segment averages calibrated against corresponding GPS signal averages, providing accurate and smoothly-varying signals with which to calculate the vehicle acceleration.

An analysis of the track grade was undertaken based on high-precision GPS signals from the CACC system that were acquired separately from those analysed in the current paper, and non-synchronously. Those data were processed to provide a long-term averaged grade profile with 1 m resolution for the outside lane of the straight segments of the track, representing the path followed through most of the testing. Correcting the road-load signals using this grade resolution introduced noise because the vehicle size acts as filter to the effects of small grade changes, along with the manner in which loads are transferred through the tires and suspension system. Using a low-pass spatial filter with a 100 m cut-off wavelength for the high-speed tests and 50 m for the low speed tests, application of the resulting grade profile was found to eliminate the changes in instantaneous road load that visually correlated with changes in the track grade.

The solution method adopted here assumes that the road load measurements at 16 km/h (10 mph) are comprised solely of rolling resistance and grade loads (no aerodynamic loads), such that

$$C_{RR0} = \frac{F_{RLi}}{W_i} \tag{15}$$

Under this assumption, the rolling resistance of the tires under the platoon test conditions can be assumed to be the same as under the isolated vehicle testing. Therefore, periodic low-speed test runs were completed throughout the test campaign with the two trucks spaced more than 1 km from each other on the track. Differences in the resulting rolling resistance coefficients were found between the north and straight segments of the track (consistently 10% higher on one side of the track than the other), assumed to be a result of the different surface conditions along the track. A near-zero-speed rolling resistance coefficient was defined by averaging the results acquired throughout the test program in the following manner:

$$\overline{C_{RR0}} = \frac{1}{N} \sum_{i=1}^{N} - C_{RR0i} \tag{16}$$

with a value defined for each tractor/trailer configuration and for each side of the track. After applying the temperature correction of Equation 9, the uncertainty on each of these rolling-resistance coefficient is on the order of 10% based on the spread of the data over the duration of the test campaign.

Using the corresponding rolling-resistance coefficient from Equation 16, the drag-area for each 600 m segment of each high-speed test run was calculated as follows:

$$C_D A_i = \frac{F_{RLi} - \overline{C_{RR0}}\ R_{RR}(V_i) W_i \left[1 + \frac{\partial C_{RR}}{\partial T}(T_i - 293) \right]}{Q_i} + \frac{\partial C_D}{\partial R_U}(R_{U,i} - 1) \tag{17}$$

For the truck-platooning tests, the on-board wind-speed measurement of the lead truck was used as the primary reference for calculating the dynamic pressure (Q, Equation 4) and wind-to-ground-speed ratio (R_U, Equation 5) for both vehicles. Each $C_D A_i$ value is also associated with a yaw angle ψ_i averaged over the same 600 m track segment, with the lead-truck value used for both vehicles for platoon test cases.

As described by McAuliffe and Chuang [14], the fidelity of the final measurements can be improved by eliminating data points for which the measurement signals varied widely during the averaging period. A similar approach was taken with the current data set. As a first step, any data point for which the root mean square (RMS) of the road load signal exceeded 5% of its mean value was removed. For any test cases for which this limit removed a significant number of data points (usually greater than 75%), a limit of 10% on the road-load RMS was imposed instead. This provided a greater number of data points from which to define the $C_D(\psi)A$ characteristics, but generally resulted in larger uncertainty estimates for the data.

A thorough uncertainty analysis has been completed to assess the accuracy of the test results from this constant-speed aerodynamic evaluation method. A conventional approach has been taken to estimate the overall uncertainty by separate assessments of the bias and random uncertainties in the measurements.

For the bias uncertainties, an error-propagation approach based on first-order Taylor-Series expansions of the principal data-reduction equations (Equations 14 and 17) has been implemented. For each of the parameters in these equations, the uncertainty in its measurement has been identified by the instrument specifications or individual measurement uncertainties. Of these, the two most dominant sources of error are the transmission efficiency ($\delta\eta = 0.02$) and the rolling-resistance coefficient as inferred by the low-speed tests ($\delta C_{RR0} = 0.0004$) which contribute to elemental sources of error on C_DA of 0.17 m^2 and 0.25 m^2, respectively. Truck 1 had an additional dominant source of error from a signal drift observed in its driveshaft-torque sensor, contributing to an elemental error on C_DA of 0.4 m^2 compared to the value of 0.04 m^2 for Truck 2.

The random uncertainties were evaluated based on statistical convergence of the individual C_DA_i values based on each 600 m test segment. Due to the anticipated and observed changes in C_DA with yaw angle, the standard error of all C_DA_i values for a given test configuration is not suitable for an uncertainty evaluation. To estimate this uncertainty, the C_DA_i data were binned with respect to the measured yaw angles ψ_i. Within the range of yaw angles observed for each test configuration, the data were associated with yaw-angle distributions of 1° increments, but calculated using bin widths of 2° (±1° from the target yaw angle). Generally, the low-yaw-angle bins contain 50 to 100 data points each (17 to 33 minutes of data per bin), with the extreme yaw-angle bins for reach test case containing anywhere from 2 to 15 data points (40 seconds to 5 minutes of data per bin). For each bin, the mean and standard error were calculated from which a C_DA and uncertainty range δC_DA were defined. The random uncertainty presented in this paper represents a 95% confidence interval.

Figure 12 shows a sample data set for the reference, isolated-vehicle, case of Truck 2. From the individual data points (grey circles) the bin averages and associated standard errors are shown with 1° increments. For cases like this, for which the test conditions can be considered symmetric or nearly-symmetric about the 0°-yaw condition, yaw-symmetric spline fits were developed. For non-symmetric conditions such as the lateral-offset platoon tests or the tests with the three-vehicle traffic arrangement, spline fits were defined based on the yaw-asymmetric data.

Once accounting for the bias-error estimates, the full confidence interval is shown as dashed lines in Figure 12. This confidence interval is relative large compared to the measurement magnitudes (±6%) and is even larger for Truck 1 (±10%). As inferred from Figure 12, the largest component of uncertainty is from the bias errors. By definition, a bias error is an error term with unknown, but consistent magnitude and offset from the measured values. Therefore, when comparing two calculated C_DA values for the same truck, the calculated difference between the two values has a much smaller uncertainty because the consistent magnitude and offset essentially cancel

FIGURE 12 Drag-area data for Truck 2 in isolated conditions.

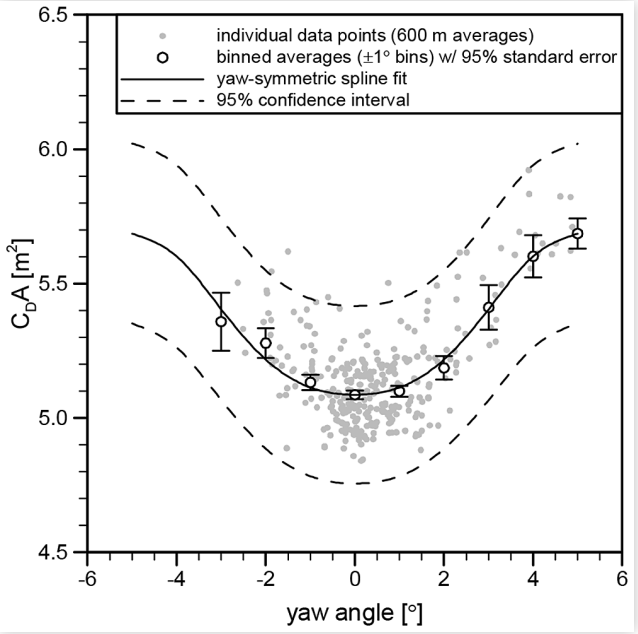

themselves between the two values. Therefore, the majority of data presented in this paper are normalized with respect to the C_DA value at 0° yaw angle of the respective truck in its isolated, non-platooning, condition. For these C_DA ratios, only the bias uncertainties that may change from test configuration to configuration, such as the rolling-resistance coefficients, the overall vehicle masses (due to fuel loss/gain), the influence of local grade changes, and the drift in driveshaft-torque for Truck 1 are retained in the uncertainty estimates, while parameters that will retain consistent bias uncertainties throughout the test such as the transmission efficiency, the dynamic-pressure and the effective mass of the wheels are neglected in the overall uncertainty estimates. For Truck 2 data in Figure 12, this process reduces the relative uncertainty magnitudes from ±6% to approximately ±2.5%. For Truck 1, the decrease in relative uncertainty is not as great, from ±10% to approximately ±8%, because the transient drift in the driveshaft-torque measurement remains.

Test Results Using the Constant-Speed Method

Reference Conditions

The reference, isolated-vehicle, conditions form the baseline against which all platoon and traffic measurements are compared. The zero-yaw drag-area values measured for each truck configuration are presented in Table 1. The drag-area values for the dry-van trailer configurations are effectively the same, within the uncertainty estimates of the measurements, and are of similar magnitude to drag-area values found in the

TABLE 1 Drag area of each truck measured for zero-yaw-angle conditions when driving in isolation.

Vehicle	Drag area, $C_DA_{0,iso}$
Truck 1 with dry-van trailer	5.3 ± 0.5 [m^2]
Truck 2 with dry-van trailer	5.1 ± 0.3 [m^2]
Truck 2 with flat-bed trailer	5.7±0.3 [m^2]

open literature for similarly-configured trucks [14, 31]. The drag area of Truck 2 with the flat-bed trailer is greater than that with the dry-van. Despite the smaller trailer volume, the lack of side-skirts and base treatment along with the bluff cargo (concrete blocks used for ballasting) lead to a zero-yaw drag-area value about 10% higher than the dry-van configuration. The sensitivity of the drag-area values with yaw angle for these three configurations are shown in Figure 13 and are presented as a ratio relative to the zero-yaw values of each truck from Table 1. The results in Figure 13 show an increase in drag-area with yaw angle, and the two dry-van-trailer configurations demonstrate a similar sensitivity with an increase in drag area upwards of 10% at yaw angles of about 5°. This is consistent with the yaw sensitivity observed for similar vehicles in other track and wind-tunnel studies [31, 40, 41]. The drag-area data for the flat-bed configuration show a lower sensitivity to yaw angle with a maximum increase of only 3% over the measured range of yaw angles, likely due to the smaller side area under cross winds. This is generally consistent with wind-tunnel data presented by McAuliffe [41] for a flat-bed configuration compared to a dry-van configuration, except for the small dip in drag-area at the highest yaw angle which is assumed to be in error due to the limited data at those larger yaw angles.

Aligned Platoon

The aligned-platoon drag-area results are presented in Figures 14 and 15 for Trucks 1 and 2, respectively. In Figure 14 it is immediately obvious that the measured differences for most of the data are within the high experimental uncertainty of the Truck 1 measurements. However, the results for most of the separation-distance cases reflect the same trends as the reference case with increasing drag-area with yaw angle. Only the 15 m separation case shows a decreasing drag-area with yaw angle, but there is very little data available for this case due to instrumentation errors during testing, as reflected in the small range of yaw angles over which data are available. Although the uncertainty bounds are large, the consistency in trends with yaw angle for most cases suggest the trends with separation-distance may be representative of the aerodynamic influence of truck platooning on a lead truck. These data show a drag-area lower than the reference case for the three closest separation distances (up to 15 m), with an increase in drag area at larger distance with similar magnitudes to the reference case. Most aerodynamic and fuel-economy studies of truck platooning demonstrate similar trends, with benefits to the lead truck occurring at distances below about 20 m separation [1, 2, 3, 7, 8, 10, 20, 21, 24].

The drag-area trends of Truck 2 differ from Truck 1 and have a smaller uncertainty, which produces greater confidence that the observed trends reflect the true aerodynamic performance of the truck platoon. Figure 15 shows that the drag-area of Truck 2 is less than the reference-case values at all separation distances tested and at all yaw angles experienced. This data reflects the general trends in fuel-consumption results for the current and other truck-platoon investigations [1, 2, 3, 7, 8, 10, 20, 21, 24]. The drag-area results for the four closest separation distances of 9 m, 12 m, 15 m, and 23 m are all

FIGURE 13 Yaw sensitivity of drag area measured for Trucks 1 and 2 under reference conditions. Gray lines show uncertainty bounds.

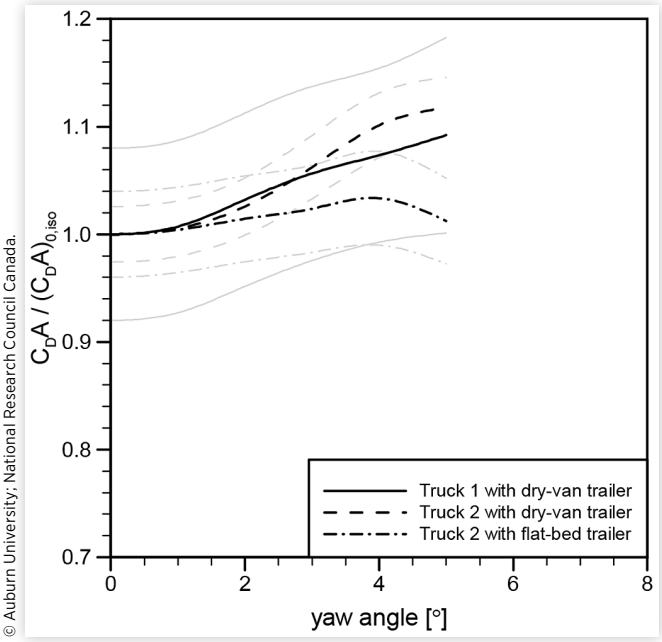

FIGURE 14 Drag-area measurements for Truck 1 in aligned-platoon formation. Gray lines show uncertainty bounds.

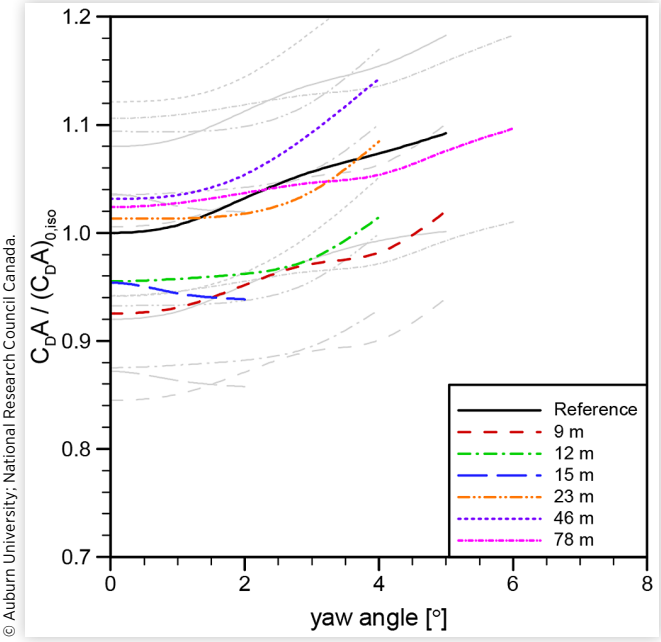

FIGURE 15 Drag-area measurements for Truck 2 in aligned-platoon formation. Gray lines show uncertainty bounds.

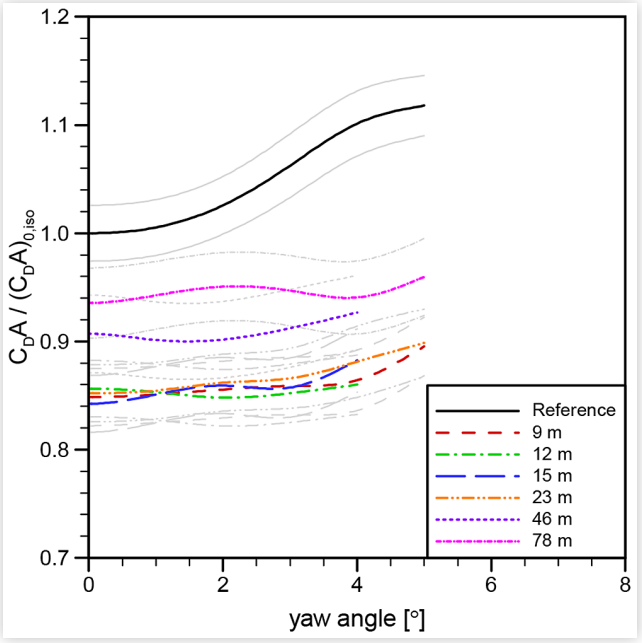

FIGURE 16 Change of drag-area measurements with separation distance for the aligned-platoon formation.

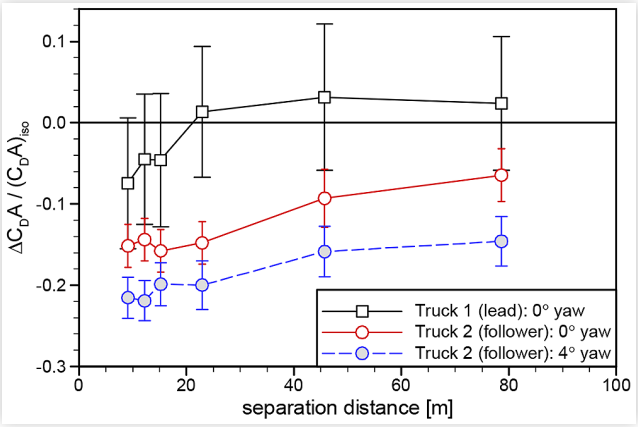

similar, with drag-area values approximately 85% of that for the isolated truck at zero yaw angle. With greater separation distance (46 m and 78 m) the drag-area increases with distance but remains lower than the reference case, at about 94% of the zero-yaw reference drag area at 78 m. Of particular interest with these measurements is the reduced sensitivity of drag area with yaw angle compared to the reference case or compared to the trends observed for the lead truck in platoon formation. This results in an increase in drag-reduction magnitude (ΔC_DA) with increasing yaw angle. A similar reduced sensitivity to yaw angle was observed in the data of McAuliffe and Ahmadi-Baloutaki [8] which, although not shown directly in this paper, can be inferred from the ΔC_D values they provide. Their data shows increasing magnitude of drag reduction with yaw angle, similar to that inferred from the data in Figure 15, with peak drag reduction around ±5°. The primary author of this paper has confirmed through a re-examination of the raw data from that study, that the trend is a result of reduced sensitivity of C_D with yaw angle up to about 5°. In the data of Figure 15, a slight increase in drag area is observed beyond about 4°, but the small proportion of data at these yaw angles prevents any conclusive statement about the manner in which the drag-area trends change with larger yaw angle in this real-world study.

To characterize the variation of drag area with separation distance, the change in drag-area values relative to the isolated-truck measurements are shown in Figure 16 for Truck 1 and Truck 2 at 0° -yaw conditions and for Truck 2 at 4° -yaw conditions. The ΔC_DA values represent the difference from the corresponding isolated-truck case at the respective yaw angle. Despite the large error bars, particularly for Truck 1, the trends reflect the trends in fuel-savings measurements documented earlier in Figure 1. The lead truck exhibits drag reduction below 20 m separation distance, and the following truck exhibits its peak drag reduction in this same range. The peak drag reduction for the following truck is on the order of 15% at 0° yaw angle and exceeds 20% at 4° yaw angle. This is similar to the 15-20% reduction observed in this range by McAuliffe and Ahmadi-Baloutaki [8] and Salari and Ortega [7] in their two-truck wind-tunnel studies. Both of those studies used wind-averaged-drag for their assessment, which provides a weighted average based on the probability of encountering a given yaw angle. Wind-averaged-drag calculation methods generally require data for yaw angles upwards of at least 7° , which are not available from the current data set. Even the surrogate ±4.5° average used in North American GHG regulations [12] as a representation of the wind-average drag value is unreliable with the current data set, due to the lack of 4.5° data from many of the test cases and due to the greater uncertainty in those higher-yaw-angle data. Despite the difference in the metric used, comparison of the general trends with separation distance between the current study and those wind tunnel studies is good.

Although the wind-speed measurements from the lead truck are used to calculate the drag area of both the lead and following trucks when in platoon formation, the corresponding measurements from Truck 2 provide insights about the changes in its drag-area with separation distance and yaw angle. Figure 17 shows the ratio of the wind speed measured by the Cobra probe of the following truck to that of the lead truck, averaged for conditions under which the yaw angle was measured to be within ±2°. At the closest separation distance of 9 m, the wind speed forward of Truck 2 is approximately two thirds of that forward of Truck 1. This reduced wind speed is a principal mechanism of the drag reduction experienced by the following vehicle in a multi-vehicle platoon. The reason for the plateau of the drag-reduction trend at separation distances of 15 m and below (in Figure 16), despite the wind speed continually decreasing as the distance is reduced, has yet to be explained adequately in the open literature.

The wind-velocity measurements from both trucks also provide some insight to explain why the drag area of the following truck in a platoon configuration demonstrates a reduced sensitivity to yaw angle over the range of yaw angles experienced, as highlighted with respect to Figure 15. Figure 18

FIGURE 17 Ratio of wind speed ratio (Truck 2 to Truck 1) with separation distance, based on forward-mounted Cobra probes (2 m from ground, 1 m forward of vehicle).

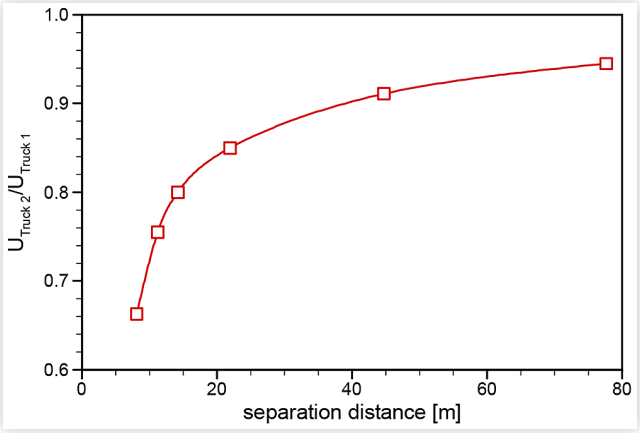

shows the correlation of yaw angle experienced by Truck 2 to that experienced by Truck 1, for the six separation distances tested. In this graph, a slope of 1 (yaw angle of Truck 2 = yaw angle of Truck 1) would indicate that the winds in the wake of Truck 1 follow the same direction as the freestream winds. The data in Figure 18 show that only at the largest separation distances (46 m and 78 m) do the winds in the wake even demonstrate the same sign as the freestream winds over the full yaw-angle range, indicating that the lead vehicle redirects the winds in the wake, effectively introducing side-wash. This is analogous to the downwash generated by a lifting wing at an angle of attack to the freestream wind [42]. At distances of 23 m and below, the yaw angles experienced by Truck 2 have the opposing direction to the freestream winds over part of the yaw-angle range, indicating side-wash of greater magnitude than the freestream yaw angle at this measurement location (2 m from the ground). In a study of the yaw-angle effects on the wakes of ground vehicles, McAuliffe, Barber and Sowmianarayanan [43] show that, under non-zero-yaw-angle conditions, a large vortex structure is generated by the vehicle under cross wind that has a dominant influence on the flow angularity near the ground, reducing the yaw angle from its freestream magnitude. Through a combination of wind-tunnel measurements and CFD simulations, they show that this vortex causes the flow near the ground to be reoriented towards the direction of motion of the vehicle. Based on wind-tunnel measurements for a heavy-duty vehicle of similar configuration to that used in the current study, at a distance behind the truck model of 18 m (full-scale distance), their measurements show that the large vortex is sufficiently strong to cause the near-ground flow to be of opposite direction to the freestream wind direction, similar to what is observed in Figure 18 for separation distances of 23 m and less. To quantify the magnitude or strength of the vortex or side-wash, the slope of the yaw-angle data from Figure 18 (based on the Truck 1 zero-yaw condition) is used as an indicator. This yaw-slope is presented in Figure 19, for which a negative values indicates a reverse orientation of the flow directionality over some range of yaw angles. As noted earlier, a yaw slope of 1 would indicate the wake flow is aligned with the freestream, while the values in Figure 19 are all well below 1 indicating a re-orientation of the wake flow, from freestream, at all separation distances tested. This reduced yaw angle, as experienced by the following truck in a two truck platoon, is likely a contribution factor to the reduced sensitivity of the drag area of Truck 2 with yaw angle shown earlier in Figure 15. Although the flow is highly three-dimensional, it can be argued that the effective yaw angle for the following vehicle is lower than that of the freestream and therefore the drag area of Truck 2 will not increase to the same magnitude as it would when encountering the corresponding freestream winds. Essentially, the following truck experiences not only a reduced wind speed when travelling in close proximity to the lead truck, but also experiences a reduced yaw angle, both effects of which lead to reduced drag of a heavy truck.

FIGURE 18 Relationship of yaw angle experienced by Truck 2 to the yaw angle experienced by Truck 1, based on forward-mounted Cobra probes (2 m from ground, 1 m forward of vehicle).

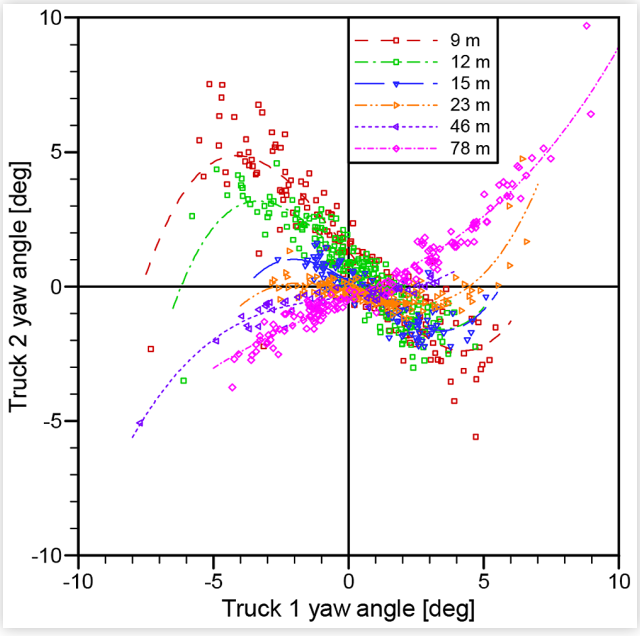

FIGURE 19 Yaw slope (zero-yaw values extracted from data in Figure 18) with separation distance.

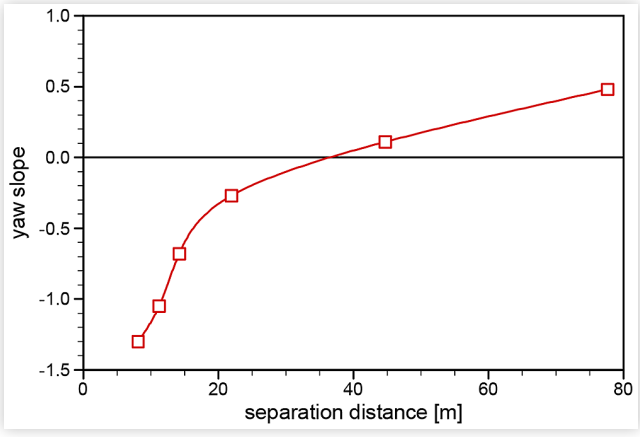

Aligned Platoon with a Flat-Bed

Drag-area data for a single platoon configuration with a flat-bed trailer are available from the data set. Figure 20 shows the results for the flat-bed attached to Truck 2, while Truck 1 is connected with a dry-van trailer, for a separation distance of 15 m. In comparison to the 15 m dry-van case in Figure 15, the zero-yaw drag-area value is slightly higher relative to the baseline truck configuration (0.88 versus 0.84) but the experimental uncertainty is sufficiently high that no conclusions can be made about differences in these zero-yaw drag-area reductions. As with the dry-van configuration, the drag area for the flat-bed in platoon formation has a low sensitivity to yaw angle over much of the yaw-angle range experienced. Although waviness to the trend is observed, with a decrease in drag-area at the highest yaw angles, similar to that observed for the isolated truck, these variations are within the experimental uncertainty and would require greater measurement accuracy to verify.

Offset Platoon

At each of the four closest separation distances (9 m, 12 m, 15 ,m, and 23 m), measurements were performed with Truck 2 laterally offset by either a quarter- or half-truck width (0.65 m or 1.3 m) in addition to the aligned configuration. The following truck was offset towards the left (towards driver side) in these tests, as shown earlier in the photographs of Figure 8. The large uncertainty associated with the drag-area data of Truck 1 make any interpretations of the influence of lateral offset inconclusive for that vehicle, and therefore the data for Truck 1 are not shown in this section. Figures 21 through 24 show the influence of lateral offset on the characteristics of drag-area of Truck 2 with yaw angle for the furthest to closest separation distances, respectively.

At separation distances of 23 m and 15 m, the data of Figures 21 and 22 show small changes in the magnitude of drag area between the aligned and offset cases, but with a difference generally within the experimental uncertainty.

FIGURE 20 Drag-area measurements for Truck 2 with a flat-bed trailer in the aligned-platoon formation. Gray lines show uncertainty bounds.

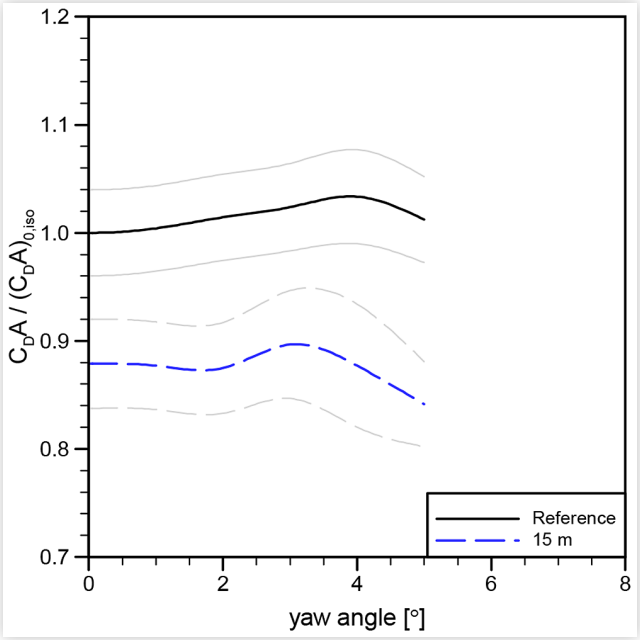

FIGURE 21 Drag-area measurements for Truck 2 in aligned- and offset- platoon formation at 23 m separation distance. Gray lines show uncertainty bounds.

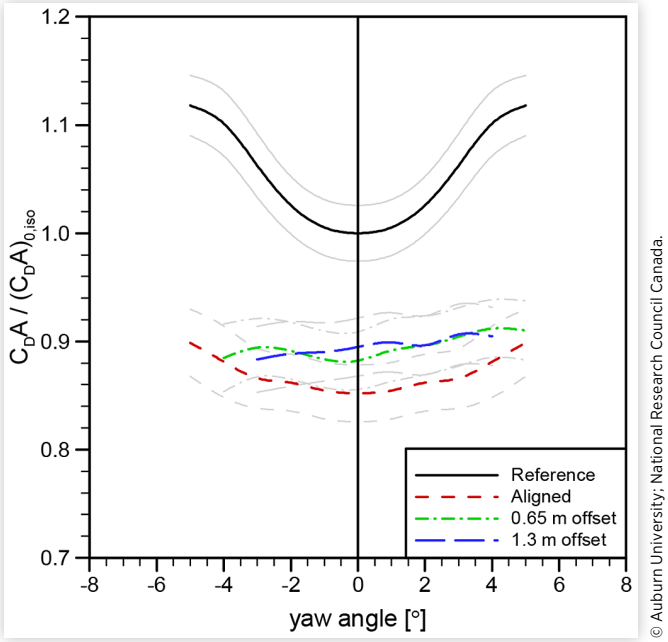

FIGURE 22 Drag-area measurements for Truck 2 in aligned- and offset- platoon formation at 15 m separation distance. Gray lines show uncertainty bounds.

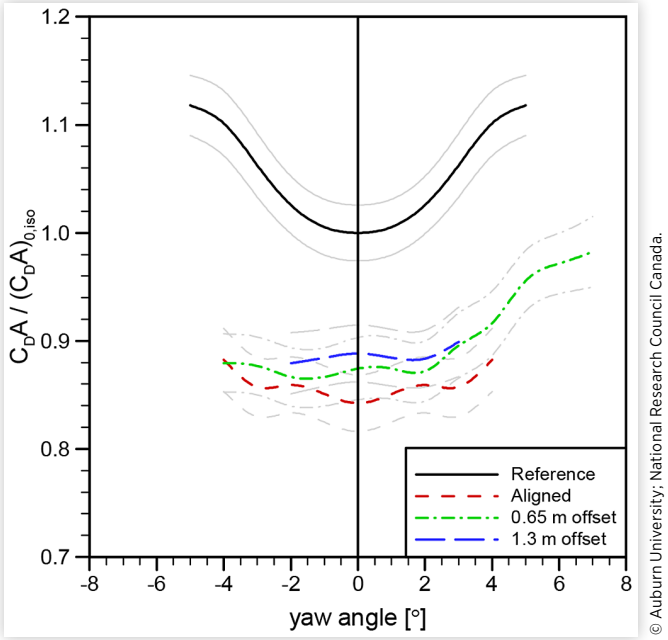

Therefore, there are no conclusive changes observed in the characteristics of drag area at these separation distances and within the range of yaw angles experienced. Drag-area data for the 15 m case show an increase at yaw angles exceeding about 4°, but there are no aligned-platoon data under these conditions against which this can be compared.

At separation distances of 12 m and 9 m, the data in Figures 23 and 24 show a distinct influence of lateral offset on the drag area of the following vehicle of the platoon. At both of these separation distances, the drag-area remains low at negative yaw angles (winds from passenger side) but increases with yaw angle at positive yaw angles (winds from driver side). Based on the direction of offset (towards the driver side), the following truck would experience greater exposure to freestream wind when encountering positive yaw angles, while the vehicle would be shielded to a greater extend by the lead truck when exposed to negative yaw angles, which corroborate the trends observed at these two separation distances.

The two wind-tunnel studies in the open literature, discussed previously, have also examined the influence of lateral offset on the aerodynamic performance of two truck platoons [7, 8]. Both studies used a wind-averaged-drag-coefficient metric for their evaluations and are therefore not directly comparable to the data of the current study, but they do provide trends that are reflected in the current data. Both studies demonstrated differences in the influence of lateral offset with different trailer configurations, while both had one configuration equivalent to the current truck configuration on the track (high-roof sleeper cab paired with dry-van trailer outfitted with side skirts and boat tails). The 1/50-scale experiments of Salari & Ortega [7], which tested offsets to the same half-trailer-width offset of 1.3 m (full scale) examined here, show approximately 4-5% increase in the wind-averaged drag coefficient for the half-width lateral offset at separation distances of 9 m and 15 m (full scale), with approximately 2% increase at the quarter-width offset for the same separation distances. At 48 m separation distance, their data show only a 1% increase in drag for a half-width offset. The 1/15-scale experiments of McAuliffe & Ahmadi-Baloutaki [8] show, for a 30%-width offset, an increase in wind-averaged-drag coefficient of about 3% at separation distances of 15 m or less, with about 1% increase at greater separation distances. That study also shows the changes in drag coefficient (ΔC_D) associated with platooning, and how they change with separation distance and lateral offset, although for a standard trailer without skirts and tail. Those data show the same trends exhibited in Figures 23 and 24 with greater changes in drag-area between the isolated truck and the platoon case at negative yaw angle than at positive yaw angle. Despite not being able to compare the current data to those wind-tunnel results directly, the aggregate fuel-savings results (see Figure 1) show a marginal reduction in benefits with lateral offset, which is the same trend observed in the wind-averaged wind-tunnel results.

FIGURE 23 Drag-area measurements for Truck 2 in aligned- and offset- platoon formation at 12 m separation distance. Gray lines show uncertainty bounds.

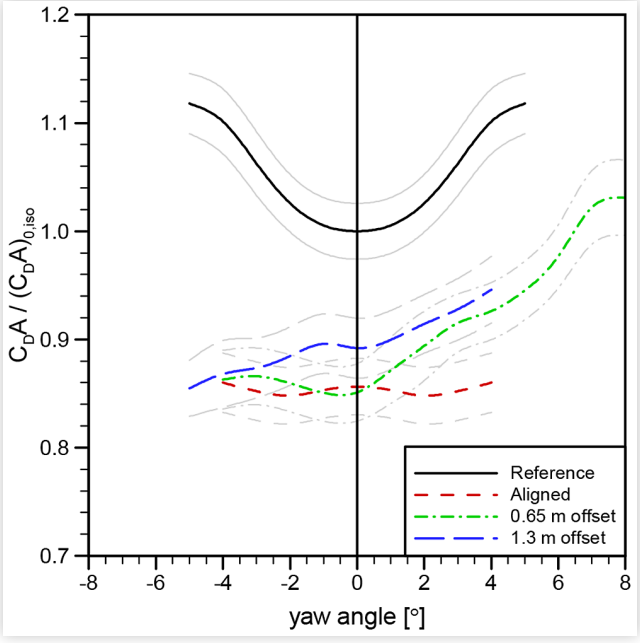

FIGURE 24 Drag-area measurements for Truck 2 in aligned- and offset- platoon formation at 9 m separation distance. Gray lines show uncertainty bounds.

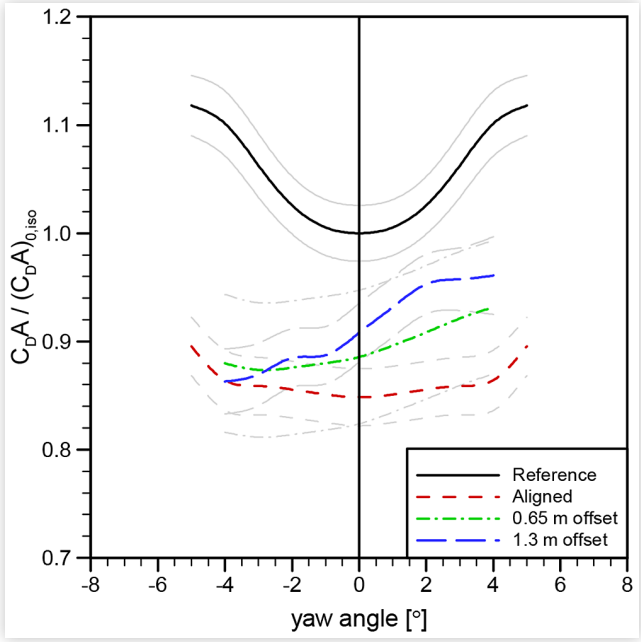

The data above demonstrate that the aerodynamic benefit of truck platooning is influenced by changes in the lateral alignment of the trucks in a platoon, particularly at the closer separation distances. The 1.3 m offset is likely not to be experienced on the road because the overall two-truck width (3.9 m) would exceed the width of a typical lane (3.7 m). However, the 0.65 m offset may be experienced on the road, whether by natural drift within the lane or by the driver of a following truck offsetting to see further ahead. Although the decrease in platoon benefit is small under these conditions, sustained operation with an offset condition could have a longer term impact on fuel savings. Furthermore, controlled offsetting

may be desired to either improve the drag-reduction benefit by optimizing the lateral position based on the freestream wind direction, or perhaps to permit greater levels of cooling flow through the engine when carrying heavy loads in hot environments.

Surrounding Traffic

To quantify the impact of surrounding traffic on the aerodynamic performance of a truck platoon, the influence of traffic on the individual trucks was first examined. Two traffic scenarios were defined: one with a single forward vehicle represented by an SUV positioned 78 m ahead of the test truck; and one with a three-vehicle multi-lane arrangement ahead of the test truck. The three-vehicle arrangement, shown earlier in Figures 9 and 10, included the same SUV as the single-vehicle configuration positioned at the same forward distance of 78 m. The two other vehicles were positioned in the adjacent lane on the driver side such that the influence of the vehicles is expected to create greater aerodynamic wake effects for the trucks at positive yaw angles than at negative yaw angles.

Figure 25 shows the drag-area results of the individual trucks from the forward-traffic tests, relative to the performance of the trucks in isolation. Truck 1 was tested with the two traffic scenarios while Truck 2 was tested only with the three-vehicle traffic. For Truck 1, the measurements show a drag reduction at 0° yaw angle of 8%, with uncertainty bands on the same order of magnitude such that the exact magnitude cannot be ascertained by the current data set. With the three-vehicle traffic scenario, the Truck 1 measurements show approximately 15% reduction, but again with a large uncertainty that prevents reliable quantification of these results. However, it can be reasonable assumed based on this data that the aerodynamic drag of Truck 1 is reduced in the presence of forward traffic. The drag-area results in Figure 25 for Truck 2 with the three-vehicle traffic show a reduction in drag area of approximately 9% at zero yaw, with much smaller uncertainty levels (±3%) compared to those of Truck 1. Despite the lower drag area measurement of Truck 1 for the same traffic scenario, the uncertainty of those measurements overlap those of Truck 2, and therefore the results for Truck 2 likely represent better the influence of the three-vehicle traffic pattern.

FIGURE 25 Drag-area measurements for Truck 1 and Truck 2 when travelling behind passenger-vehicle traffic. Gray lines show uncertainty bounds.

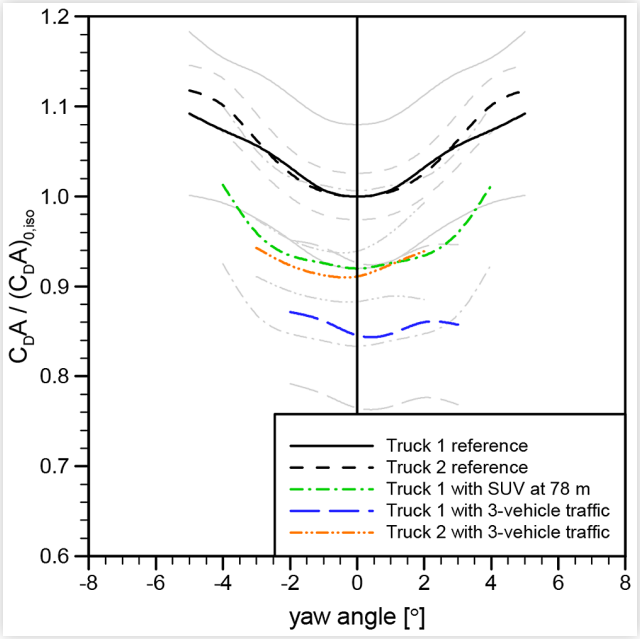

The multi-vehicle traffic results of Figure 25 show data acquired over a smaller range of yaw angles than many of the other data sets. This is also the case for many of the platoon-in-traffic cases presented in the next section. For these "forward traffic" test cases, the high-mount Cobra probe on Truck 1 was used as the primary wind-speed reference, properly calibrated against the track-side anemometers, as opposed to the forward mounted probe used when other vehicles were not present. At 5 m height from the ground, this probe was expected to be negligibly influenced by the wakes of the forward traffic, based on wind-tunnel and CFD results like those presented by McAuliffe, Barber and Sowmianarayanan [43, 44, 45]. However, the results of the current data indicate that the wind-speed at this location measured lower than would be expected in the presence of forward traffic. This was identified by examining data from test cases for which the ambient winds were low and were aligned with the direction of motion of the vehicle on the straight segments of the track. For each lap of these cases, the calibrated wind-speed values were averaged between the north- and south-side straight segments. Without forward traffic, these averages were the same as the vehicle ground speed, within about ±1%, while when following other traffic these averages were consistently lower than the vehicle ground speed by about 1-3%, indicating that the high-mount probe is influenced by wake effects. It is unclear whether the wakes of the forward traffic expand to greater heights than predicted, or whether the interaction of the wakes with the truck cause the wake flow to be directed over the top of the vehicle, but clearly the wakes influence the wind-speed calibration of the high-mount probe. The wakes may then also be influencing the yaw-angle calibration of this probe. If this is the case, then the results discussed earlier with respect to the effect of the lead-truck wake on the flow angularity forward of the following truck suggest that the high-mount probe may be measuring a lower yaw angle than that of the freestream winds. A correction for wake effects was made to the reference wind-speed measurements, based on the quantifiable influence. However, such a correction was not possible for the yaw-angle measurements. The surrounding traffic results should therefore be examined in this context, with the perspective that the true yaw angles may be greater than those indicated.

Aligned Platoon with Surrounding Traffic

The two-truck platoon was tested at five separation distances in the presence of the three-vehicle traffic pattern. As with many of the earlier test results presented in this paper, the high uncertainty of the data for Truck 1 make any

interpretations more challenging. Therefore, results are presented here only for Truck 2. Figure 26 shows drag reductions associated with the combined effect of forward traffic and platooning exceeding 20% for the range of yaw angles encountered. With respect to the truck-in-traffic reference case, the 0° -yaw drag-area trends for the platoon cases appear similar to those presented earlier in Figure 15 for the aligned truck without forward traffic. The main difference here is lower drag-area measured at positive yaw angles than at negative yaw angles. As noted earlier, this is expected based on the wakes of the vehicle in the driver-side adjacent lane having a greater likelihood of interaction with the trucks at positive yaw angles.

The change in drag area with separation distance of Truck 2 at 0° yaw angle is shown in Figure 27 for the standard aligned-platoon case (black squares) and for the platoon-in-traffic case (red circles and blue triangles). Using the isolated truck as a reference for the platoon-in-traffic data (red circles), the data show drag reductions in excess of 20% at separation distances of 23 m or less, resulting from the combination of forward traffic and platooning. Using Truck-2-in-traffic as the reference for this data (blue triangles), the magnitude of platoon drag reductions at these shorter distances are similar to what was measured for the standard aligned platoon, while at the longer separation distances the drag reductions in traffic are lower than those without forward vehicles. However, these differences are within the experimental uncertainty of the two data sets preventing any conclusive arguments regarding the influence of surrounding of surrounding traffic at these separation distances. These results are in contrast to what was found with the simultaneous fuel-economy measurements [3] where the shorter distances showed lower savings in traffic and the longer distances showed similar savings. Although,

FIGURE 26 Drag-area measurements for Truck 2 in aligned-platoon formation when travelling behind the three-vehicle traffic pattern. Gray lines show uncertainty bounds.

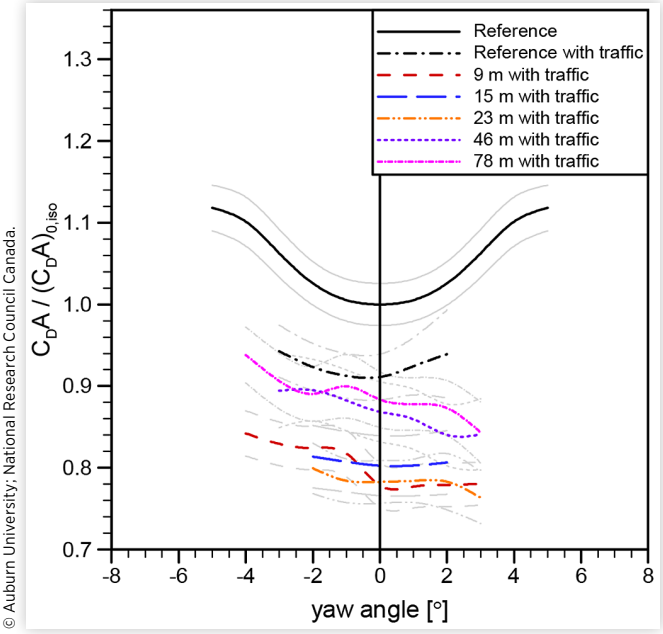

FIGURE 27 Change of the 0°-yaw drag-area measurements of Truck 2 with separation distance for the platoon-in-traffic formation compared to the isolated-platoon formation, relative to the respective reference drag-area measurements.

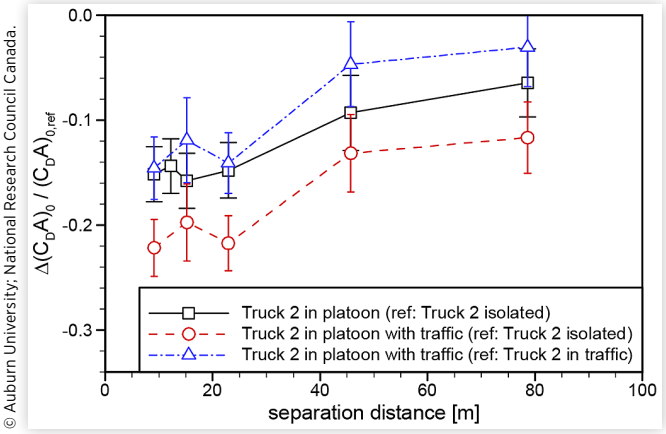

like the current data set, the uncertainty bars for the fuel-savings measurements overlap for most of those cases so definitive conclusions cannot be made from them either. An important take-away from these results are that the trends of truck-platoon drag reduction and fuel savings are retained when travelling with traffic forward of the lead vehicle, while differences in the magnitudes require greater accuracy in the measurements.

Coast-Down Proof-of-Concept Study

In addition to constant-speed analysis, coast-down testing is another experimental aerodynamic evaluation method. As previously mentioned, the coast-down test is the reference aerodynamic evaluation method in North America [12], and this method has been previously applied to single heavy duty trucks [14, 46, 47, 48]. In particular, Hausberger et al. [46] and McAuliffe and Chuang [14] completed both coast-down and constant-speed testing and compared the results. The tractor-trailer drag area results in [14] showed the two test methodologies were within 1%, which demonstrates these two methods produce comparable results.

In current literature, there are few studies that apply these aerodynamic evaluations to platooning vehicles. The most recent studies were completed by Duoba and Fernandez Canosa [49] who completed constant-speed testing for a platoon of two sedans and McAuliffe [25] who documented constant-speed analysis for a three-truck platoon as part of similar fuel-economy study. These prior studies, along the constant-speed results of the current paper, demonstrate the differing aerodynamic forces on leading and following platoon vehicles. In the context of a coast-down test, the differing forces on these vehicles results in a constantly changing separation distance which that must be controlled for a valid result. For the constant-speed testing in [49], the gap distance was controlled manually by a driver, and a CACC system was used for the constant-speed testing in [25].

In this section, a novel approach is demonstrated to apply the coast-down test method for platooning vehicles. This approach, the "controlled" coast-down, makes use of a CACC system to maintain the desired gap distance while the other vehicle coasts down. Despite limitations in the setup with respect to conventional heavy-truck coast-down testing, including proper test speeds and a lack of wind instrumentation, this study demonstrates the viability of the coast-down method to analyze truck platooning.

Test Vehicles

The controlled coast-down was applied to the same two-truck platoon used for the fuel-consumption and constant-speed-aerodynamic measurements, but during a separate test campaign. The two tractors were configured similarly to the other tests, with the main difference being the use of unloaded dry-van trailers. The unloaded trailers (Hyundai Translead models for this study) were outfitted with trailer side skirts but lacked the boat-tails used in the other study. As a result, the absolute drag area results presented here are expected to be nominally higher than the drag experienced during the fuel test. The test-truck configuration for this study is shown in Figure 28. The vehicle mass was approximately 14,000 kg (31,000 lb), which is less than 50% of the vehicle mass previously tested.

Testing was completed with Truck 1, typically the platoon lead vehicle for all prior testing, as the coast-down test vehicle. Truck 1 was operated in three different configurations: the reference case, the regular platoon, and the inverted platoon. The reference, or single vehicle, case was completed with Truck 1 operating in isolation, i.e. not platooning. The single-vehicle test provides the baseline drag area for comparison to the platooning configurations.

CACC System

The CACC system was used to maintain the desired gap distance during the coast-down testing. As previously mentioned, it is necessary to control the gap distance in the coast-down configuration because of the differing coast-down rates from aerodynamic drag reduction. Truck 1 was the coast-down vehicle throughout testing, and Truck 2 was the controlled vehicle, or the vehicle operating under CACC control.

In order to quantify the drag-area reductions from platooning, Truck 1 must operate in both the lead and following vehicle positions for respective tests. The coast-down testing included two different platoon configurations: the lead vehicle position, or "regular" platoon, and the following vehicle position, or "inverted" platoon. The term "regular" platoon describes that the CACC system is operating as it was originally designed: the lead vehicle is operated manually and the following vehicle is controlled. This configuration is the same used in the fuel-consumption and constant-speed testing. For coast-down testing, the CACC system operates on the following vehicle and maintains the desired gap distance to the lead vehicle through throttle or braking commands as the leader coasts.

FIGURE 28 Truck configuration for coast-down tests.

FIGURE 29 Regular platoon configuration to quantify the lead vehicle's drag reduction.

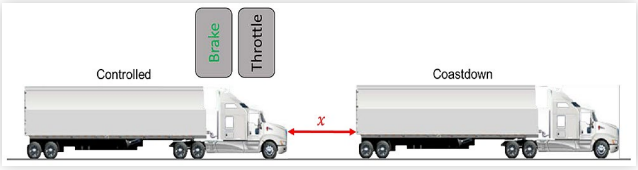

FIGURE 30 Inverted platoon configuration to quantify the following vehicle's drag reduction.

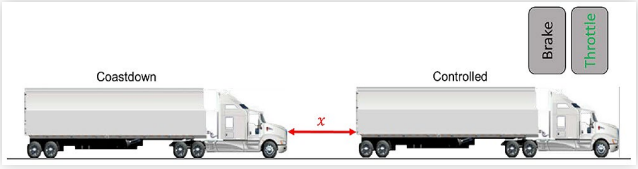

The drag area reductions of the following vehicle position are achieved by inverting the controlled and coast-down vehicles. In this case, Truck 1 is still the coast-down vehicle but is the platoon following vehicle. The CACC system operates on Truck 2 in the lead vehicle position and controls the gap distance to the vehicle behind. This configuration required modification to the CACC system measurements and control system, which is covered by Smith [50]. The regular and inverted platoon configurations are shown in Figures 29 and 30 respectively.

Test Site

The coast-down testing was completed at Auburn University's National Center of Asphalt Technology (NCAT) test track. The test track is a 2.7 km (1.7 mile) oval and is typically used for testing a variety of asphalt mixes. The inside lane of the track was used for testing, and only the straight segments of the track were used for testing due to the high degree of bank in the turns. The straight segments of the track are approximately 0.8 km (0.5 miles) long.

The biggest limitation of the NCAT test track for coast-down testing is the speed limit. Typically, a starting speed over 113 km/hr (70 mph) is desired for a coast-down test, but the track speed limit is 76 km/hr with a loaded truck. This testing was completed with unloaded trailers so that the vehicles could operate at a higher start speed of 89 km/hr.

Measurements

The coast-down analysis method implemented here only requires measurements of position, velocity, and time. The position and time information was collected using a GPS receiver, and the velocity information was collected from the vehicle's CAN bus, and the data were collected on-board Truck 1 with a passive CACC system. Additional information was also collected from the vehicle to help with post-processing of the data. This information included brake and gear selection data that was used to monitor and verify successful tests. For example, the start of a coast-down test was signalled when the current gear was in neutral.

Environmental conditions were monitored track-side by a weather station (Airmar 220WX model). The weather station collected temperature and atmospheric pressure data that was used to correct the local air density for a given day. These data were aligned with the vehicle data using GPS time.

Test Procedures

The test procedure was derived from SAE J1263 [51], SAE J2263 [52], and the Environmental Protection Agency's (EPA) Greenhouse Gas (GHG) Phase I and II documents [12, 53]. These documents provided a basis for the testing and evaluation described herein. This test campaign utilized a split range coast-down due to track length and speed constraints. A split range coast-down differs from a traditional one because the deceleration is broken up into segments rather than being continuous. The split range is ideal for test tracks with length constraints where it is not possible to coast from the high to low speed in a single segment.

The target speeds for the high- and low-speed segments were selected as 89 to 72 km/hr (55 to 45 mph) and 24 to 8 km/hr (15 to 5 mph), respectively. The high- and low-speed segments were always completed on the same side of the track (i.e high speed on the south straight, low speed on the north straight) for consistency. A single coast consisted of one high-speed segment followed immediately by a low-speed segment. Multiple coast-down tests were completed consecutively (e.g. four tests in a row) and then the same tests were repeated traveling in the opposite direction of the track. The coast-downs were completed in both track directions in order to minimize environmental effects, average out road grade, and help remove outliers. In particular, this testing ignores the effect of local wind conditions which can have a significant impact, as discussed in the constant-speed analysis section. It is assumed that traveling in opposite directions of the track effectively cancels out the wind vector the vehicle or platoon experienced.

Coast-Down Analysis

The concept of the coast-down analysis is to infer the external forces acting on a vehicle from the deceleration rate when coasting un-powered. The coast-down equation of motion is similar to that of Equation 1 and is shown as

$$m_e \frac{dv}{dt} = -F_{aero} - F_{RR} - F_{mech} - F_{grade} \tag{18}$$

for which the force components (F_i) in the equation are defined the same as those previously described earlier in the paper (Equations 3, 9 and 12), with the exception of the mechanical resistance, F_{mech}. For lack of having a tractive force with its associated driveline efficiency, the mechanical resistance here is simply another way to model the resistive forces associated with the rotational losses of the vehicle driveline when coasting un-powered. In the coast-down analysis, models of the resistive forces are used and the deceleration rate (dv/dt) is measured.

The specific models used in this analysis also differ slightly from the constant-speed models. The models used here are the same as presented by McAuliffe and Chuang [54], including the F_{mech} term, which were applied to a similar tractor-trailer configuration.

The aerodynamic and grade forces from 1 are combined with the rolling resistance and mechanical force models of McAuliffe and Chuang [54] to form the full equation of motion as

$$QC_D(\psi)A + C_{RRO}R_{RR}(v) \times W = -m_e \frac{dv}{dt} - F_{mech}(v) - W\frac{dh}{ds} \tag{19}$$

where the drag area and the near-zero velocity component of rolling resistance are the parameters of interest and are arranged on the left hand side of the equation. It is important to note that, for the current coast-down analysis, the relative wind speed of the aerodynamic force (U) is assumed to be the vehicle speed without properly accounting for wind anemometry. With this assumption, the resulting drag-area value is inferred to be the zero-yaw value even though it may represent conditions with winds.

Equation 19 is solved using the segmented analysis method, similar to that used for the North-American GHG regulations [12] and by the SAE J2978 procedure [55]. McAuliffe and Chuang [14] refer to this method as the high-low method since it uses data acquired at a high and at a low speed range, and it is the same solution approach adopted for the North American GHG regulations [12]. This method approximates the instantaneous speed derivative of Equation 19 with an aggregate deceleration during each segment, or speed range:

$$\frac{dv}{dt} \approx \frac{\Delta v}{\Delta t} \tag{20}$$

with Δ values representing the change over the respective speed range. Applying these calculated decelerations for each speed-range segment of a test run, Equation 19 results in a system of two equations with two unknowns ($C_D(\psi)A$ and C_{RRO}) which are easily solved.

Results Using the Coast-Down Method

The single, isolated vehicle case is used to quantify the baseline drag-area to which the platooning results can be compared. A total of 22 coast-down tests (11 in each track direction) were completed with Truck 1 in the single vehicle configuration.

The single-vehicle coast-down results are shown in Figure 31, where the first half of the run numbers are the clockwise track direction and the second half are counter-clockwise runs. The individually-calculated values for each run are shown as points and the solid line represents the running average. Despite some scatter, the results are consistent regardless of track direction. The resulting baseline drag area was calculated as 5.5 ± 0.8 m^2, and this value is close to the Truck 1 constant-speed result of 5.3 ± 0.5 m^2. Although the confidence intervals of these measurements overlap, the constant-speed results are expected to be lower due to the aerodynamic technology on the trailer during that test campaign (side-skirts + boat tails) compared to this one (side-skirts only).

In this proof-of-concept study, two separation distances were selected to study the platoon aerodynamic performance, with both trucks laterally aligned. The separation distances selected were 15 m (50 ft) and 46 m (150 ft) and were selected based on the fuel-economy results from [2] and reproduced as Figure 1 in the introduction of this paper. For example, at 15 m distance there was a measurable fuel savings for both lead and following platoon vehicles, but a saving was measured only for the following vehicle at 46 m. This is also consistent with the constant-speed results presented earlier in Figure 16.

The results were first evaluated for the coast-down in the lead vehicle position, and Figure 32 shows the drag-area results at the two separation distances. It is important to note the figure's legend describes the vehicle position and the platoon gap distance, e.g. LV-S50 represents the lead vehicle coast-down position and the 50 ft (15 m) separation distance. As shown in the figure, there are fewer test runs in the lead vehicle position than acquired for the baseline configuration. This was due to time constraints and placing priority on the following-vehicle tests. These results show the drag-area results are similar for both gap distances when compared to the baseline.

The results for the inverted platoon, with the coast-down vehicle in the following-vehicle position, are shown in Figure 33. In contrast to the lead vehicle results, this plot shows a distinct reduction in the drag-area for both platoon gap distances, which is consistent with the expected magnitude difference in the respective vehicle positions. This distinction is clear despite the increased scatter in the results based on the track direction. The scatter may be due to the increased variability in the inverted control system or due to un-modeled environmental effects such as the wind [50].

The individually-calculated results were combined to examine the overall drag-area reductions from platooning. The drag-area reductions as a function of platoon separation distance are shown in Figure 34, contrasted with those measured from the constant-speed tests. For the lead vehicle, the coast-down results align well with the constant-speed results, at 15 m and 46 m, despite the large uncertainty values of each data set. As noted earlier, the platoon following vehicle has much higher reductions in the drag-area from following in the lead vehicle's wake. The following vehicle drag-area reductions were calculated to be 23 ± 7% and 17 ±° 5% at 15 m and 46 m, respectively. These drag-area reductions compare more favourably with the 4°-yaw-angle constant-speed results than with the 0° results which the coast-down results are intended to represent. The significant scatter in Figure 33, especially the differences from one track direction to the other, is an indicator that the winds were much stronger for the following-vehicle coast-down tests than for the lead-vehicle or baseline tests. The similarity of

FIGURE 31 Single vehicle baseline coastdown test results.

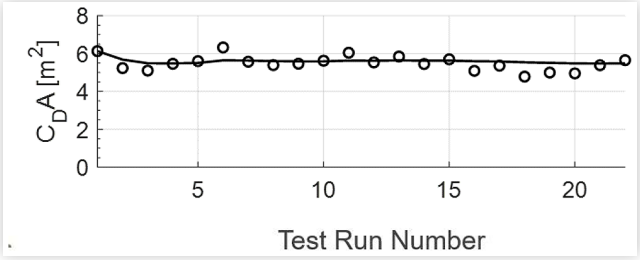

FIGURE 32 Platoon lead vehicle drag area results.

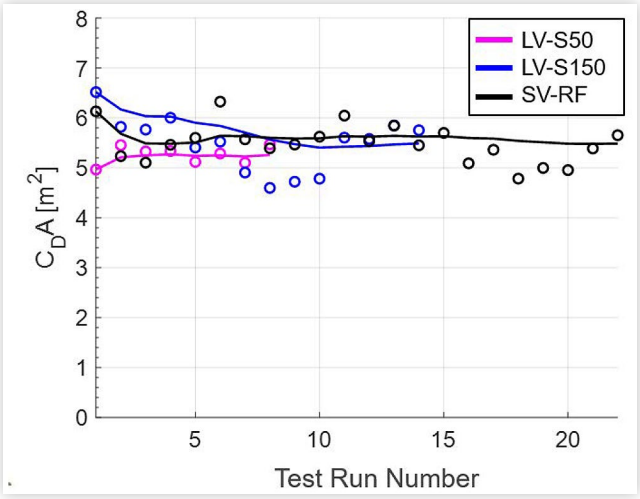

FIGURE 33 Platoon following vehicle drag area results.

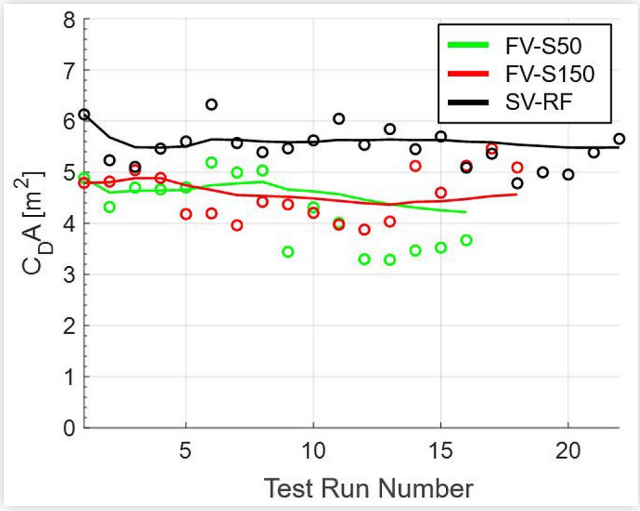

FIGURE 34 Comparison of platoon drag-area reductions measured from constant-speed and coast-down test methods.

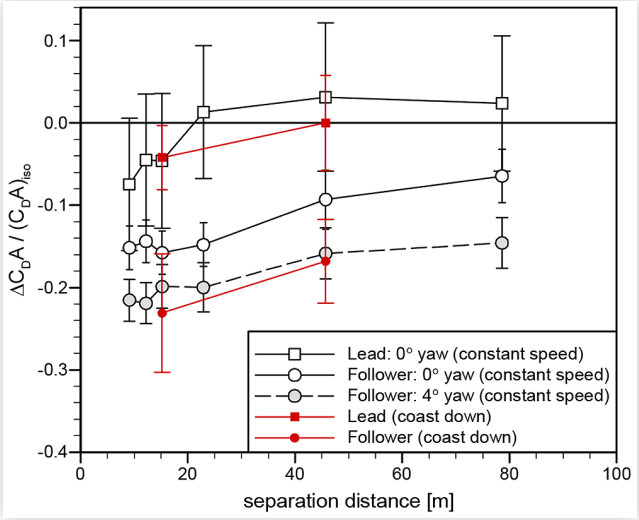

the test results to the 4°-yaw-angle constant-speed data may be another indicator of this condition. Despite the reasons for the differences, the general similarity of this data set of coast-down results, which fall within the uncertainty bounds of the respective measurements, suggests that the novel coast-down technique applied here for a two-truck platoon is a suitable approach to measure the drag-area performance of platooning vehicles. The inclusion of wind measurements and an increase in test runs are expected to improve the accuracy of these test results.

Conclusions

Track-based measurements of the aerodynamic drag of a two-truck platooning system were undertaken using two methods: the constant-speed aerodynamic test method and the coast-down test method. To reduce the uncertainty in the test results, the implementation of the constant-speed method accounted for speed-and-temperature-variable rolling resistance, calibrated on-board wind measurements, inertial-load corrections, and ground-effect corrections. A proof-of-concept coast-down test method was demonstrated that makes use of the CACC of one vehicle system to match the coast rate of the other, whether in the lead or following position. Despite some limitations in the implementation, including the absence of wind measurements, the coast-down method demonstrated reasonably-good agreement with the constant-speed test results, and is therefore demonstrated to be a viable option for such testing.

For the constant-speed aerodynamic measurements, instrumentation issues with the driveshaft of the lead truck resulted in large uncertainty in its test results, and therefore limited data was presented for the lead truck. Despite the greater uncertainty, the drag-area magnitudes and trends with yaw angles were similar for both the lead and following trucks when operated in isolation of each other.

In platoon formation, the close-distance platooning cases (separation distances of 23 m and less) showed similar levels of drag-area reduction for the following vehicle over the range of yaw angles observed on the track. At near-zero yaw angles, the drag area was reduced by about 15% at these separation distances, with drag-area reductions of 10% and 6% at the larger distances of 46 m and 78 m, respectively. Over the range of yaw angles observed during the test runs (up to about ±4°), the yaw sensitivity of the following truck was reduced compared to the isolated truck. Measurements from the forward-mounted on-board wind sensor suggest that the drag reduction and the reduced sensitivity to yaw angle are due to a combined effect of reduce apparent wind speed and reduced effective yaw angle in the wake of the lead truck. The reduced sensitivity to yaw angle leads to increased drag-area reductions of 20% at the higher observed yaw angles of ±4°.

The lateral-offset platoon cases showed that drag-area reduction is affected more so at yaw angles for which the following vehicle exhibits greater exposure to the freestream winds, while the drag area at shielded yaw angles are of similar magnitude to the aligned-platoon cases. For equal probability of winds from either side, this reduces the effective drag-area reduction of a two-truck platoon, which corroborates wind-tunnel results in the open literature that show marginal increases in wind-averaged drag under offset conditions.

With upstream passenger-vehicle traffic, drag-area reductions on the order of 10% were observed. When platooning in this traffic scenario, the following truck exhibited drag-area reductions in excess of 20% for the combined effect of traffic and platooning, relative to an isolated truck. The aerodynamic platooning benefit was shown to be retained when travelling with upstream traffic.

The results of the aerodynamic-drag-area measurements presented herein corroborate the trends of fuel-savings measurements performed simultaneously and reported in previous work, providing further evidence that aerodynamic drag reduction is the primary energy-savings mechanism of truck platooning systems when travelling at constant speed.

Acknowledgements

The work by the researchers from the National Research Council Canada (NRC) was funded by Transport Canada's ecoTECHNOLOGY for Vehicles program and by NRC's Fleet Forward 2020 program. The views and opinions of authors expressed herein do not necessarily state or reflect those of Transport Canada.

The work by researchers from Auburn University was funded by the U.S. Department of Transportation - Federal Highway Administration under contract No. DTFH61-13-H-00019.

The authors would like to thank the staff from all the organizations that provided support to the project, including:

- Transport Canada Innovation Centre, with project oversight by Marc Belzile and Pierre Villemure, and with track support led by Dominique-Pierre Dion

- NRC project management by David Poisson, with track support by David Chuang, Mark Croken, and Sheldon Harrison
- Auburn University GPS & Vehicle Dynamics Laboratory, with contributions of Jacob Ward, Evan Stegner, Christian Campos-Vega, and Dan Pierce
- FP Innovations PIT group, with track support led by Steve Mercier
- PMG Technologies, with track support led by Claude Sauvageau and Gilles Marleau
- Drivers supplied by Centre de Formation du Transport Routier de Saint-Jérome
- Drivers and staff of the National Center for Asphalt Technology (NCAT) test track

References

1. McAuliffe, B.R., Lammert, M., Lu, X., Shladover, S. et al., "Influences on Energy Savings of Heavy Trucks Using Cooperative Adaptive Cruise Control," SAE Paper 2018-01-1181, 2018, https://doi.org/10.4271/2018-01-1181.
2. Lammert, M.P., McAuliffe, B.R., Raeesi, A., Smith, P. et al., "Impact of Lateral Alignment on the Energy Savings of a Truck Platoon," SAE Paper 2020-01-0594, 2020, https://doi.org/10.4271/2020-01-0594.
3. McAuliffe, B.R., Raeesi, A., Lammert, M.P., Smith, P. et al., "Impact of Mixed Traffic on the Energy Savings of a Truck Platoon," SAE Paper 2020-01-0679, 2020, https://doi.org/10.4271/2020-01-0679.
4. Smith, J., Mihelic, R., Gifford, B., and Ellis, M., "Aerodynamic Impact of Tractor-Trailer in Drafting Configuration," *SAE Int. J. Commer. Veh.* 7(2), 2014, https://doi.org/10.4271/2014-01-2436(2014-01-2436).
5. Mihelic, R., Smith, J., and Ellis, M., "Aerodynamic Comparison of Tractor-Trailer Platooning and A-Train Configuration," *SAE Int. J. Commer. Veh.* 8(2)(2015-01-2897), 2015, https://doi.org/10.4271/2015-01-2897.
6. Ellis, M., Gargoloff, J.I., and Sengupta, R., "Aerodynamic Drag and Engine Cooling Effects on Class 8 Trucks in Platooning Configurations," *SAE Int. J. Commer. Veh.* 8(2), 2015, https://doi.org/10.4271/2015-01-2896(2015-01-2896).
7. Salari, K. and Ortega, J., "Experimental Investigation of the Aerodynamic Benefits of Truck Platooning," SAE Technical Paper 2018-01-0732, 2018, https://doi.org/0.4271/2018-01-0732.
8. McAuliffe, B.R. and Ahmadi-Baloutaki, M., "A Wind-Tunnel Investigation of the Influence of Separation Distance, Lateral Stagger, and Trailer Configuration on the Drag-Reduction Potential of a Two-Truck Platoon," *SAE Int. J. Commer. Veh.* 11(2):125-150, 2018, doi:10.4271/02-11-02-0011.
9. Humphreys, H.L., Batterson, J., Bevly, D., and Schubert, R., "An Evaluation of the Fuel Economy Benefits of a Driver Assistive Truck Platooning Prototype Using Simulation," SAE Paper 2016-01-0167, 2016, https://doi.org/10.4271/2016-01-0167.
10. Humphreys, H.L. and Bevly, D., "Computational Fluid Dynamic Analysis of a Generic 2 Truck Platoon," SAE Paper 2016-01-8008, 2016, https://doi.org/10.4271/2016-01-8008.
11. Siemon, M., Smith, P., Nichols, D. et al., "An Integrated CFD and Truck Simulation for 4 Vehicle Platoons," SAE Paper 2018-01-0797, 2018, https://doi.org/10.4271/2018-01-0797.
12. U.S. Environmental Protection Agency and U.S. Department of Transportation, "Greenhouse Gas Emissions Standards and Fuel Efficiency Standards for Medium- and Heavy-Duty Engines and Vehicles - Phase 2," *US Federal Register* 81(206):73478-74274, 2016.
13. European Commission, "Commission Regulation (EU) 2017/2400," *Official Journal of the European Union*, 2017.
14. McAuliffe, B.R. and Chuang, D. "Coast-Down and Constant-Speed Testing of a Tractor-Trailer Combination in Support of Regulatory Developments for Greenhouse Gas Emissions," NRC Report LTR-AL-2016-0019-R, National Research Council Canada, 2016.
15. Delgado, O., Rodriguez, F., and Zacharof, N. "Comparison of Aerodynamic Drag Determination Procedures for HDV CO2 Certification," Technical Report, The International Council on Clean Transportation (ICCT), 2019.
16. Bonnet, C. and Fritz, H., "Fuel Consumption Reduction in a Platoon: Experimental Results with Two Electronically Coupled Trucks at Close Spacing," SAE Paper 2000-01-3056, 2000.
17. Browand, F., McArthur, J., and Radovich, C. "Fuel Saving Achieved in the Field Test of Two Tandem Trucks," California PATH Research Report UCB-ITS-PRR-2004-20, 2004.
18. Al Alam, A., Gattami, A., and Johansson, K.H. "An Experimental Study on the Fuel Reduction Potential of Heavy Duty Vehicle Platooning," in *13th International IEEE Annual Conference on Intelligent Transportation Systems*. Madeira Island, Portugal, 2010.
19. Roeth, M. "CR England Peloton Technology Platooning Test Nov. 2013," North American Council for Freight Efficiency (NACFE), Peloton, 2013.
20. Lammert, M., Gonder, J., Kelly, K., Salari, K. et al. "Class 8 Tractor Trailer Platooning: Effects, Impacts, and Improvements," Technical Report NREL/PO-5400-66766, Automated Vehicle Symposium, San Francisco, CA, July 19-21, 2016.
21. Tsugawa, S. "Results and Issues of an Automated Truck Platoon within the Energy ITS Project," in *2014 IEEE Intelligent Vehicles Symposium (IV)*, June 8-11, Dearborn, MI, 2014.
22. Roberts, J., Mihelic, R., Roeth, M., and Rondini, D. "Confidence Report on Two-Truck Platooning," Technical Report, North American Council for Freight Efficiency (NACFE), 2016.
23. McAuliffe, B.R., Ahmadi-Baloutaki, M., Croken, M., and Raeesi, A. "Fuel-Economy Testing of a Three-Vehicle Truck Platooning System," NRC Report LTR-AL-2017-0008, National Research Council Canada, 2017.

24. Bevly, D., Murray, C., Lim, A., Turochy, R. et al. "Heavy Truck Cooperative Adaptive Cruise Control: Evaluation, Testing, and Stakeholder Engagement for Near Term Deployment: Phase Two Final Report," Tecnical Report FHWA-, Auburn University, 2017.
25. McAuliffe, B.R. "Aerodynamic Drag Reduction of Heavy Trucks Using a Cooperative Adaptive Cruise Control System," in *SAE Commercial Vehicle Engineering Congress Presentation 18-AERO-0006*, 2018.
26. Smith, P. and Bevly, D., "Analysis of On-Road Highway Testing for a Two Truck Cooperative Adaptive Cruise Control (CACC) Platoon," SAE Paper 2020-01-5009, 2020, https://doi.org/10.4271/2020-01-5009.
27. Smith, P., Ward, J., Pierce, J., Bevly, D. et al. "Experimental Results and Analysis of a Longitudinal Controlled Cooperative Adaptive Cruise Cruise (CACC) Truck Platoon," in *Dynamic Systems and Control Conference 2019*. 2019.
28. SAE J1321, "Fuel Consumption Test Procedure - Type II," *Surface Vehicle Recommended Practice J1321*, 2012.
29. Hooper, J.D. and Musgrove, A.R., "Reynolds Stress, Mean Velocity, and Dynamic Static Pressure Measurements by a Four-Hole Pressure Probe," *Exp. Therm. Fluid Sci.* 15:375-383, 1997.
30. Tanguay, B., "A Novel Technique to Optimize the Prediction of Free-Stream Velocity from Ground-Based Anemometric Measurements," *SAE Int. J. Commer. Veh.* 9(2), 2016, https://doi.org/10.4271/2016-01-8023.
31. Gururaja, P., "Wind-Averaged Drag Determination of Heavy-Duty Vehicles from On-Road Constant-Speed Torque Tests," SAE Paper 2016-01-8153, 2016, https://doi.org/10.4271/2016-01-8153.
32. McAuliffe, B.R., "The Influence of Wheel and Ground Effects on the Aerodynamic Drag of a Tractor-Trailer Combination," in *SAE Commercial Vehicle Engineering Congress Presentation 17CVA-0019*, 2017.
33. Wood, R., "Reynolds Number Impact on Commercial Vehicle Aerodynamics and Performance," *SAE Int. J. Commer. Veh.* 8(2), 2015, https://doi.org/10.4271/2015-01-2859.
34. Leuschen, J., "Considerations for the Wind Tunnel Simulation of Tractor-Trailer Combinations: Correlation of Fulland Half-Scale Measurements," *SAE Int. J. Commer. Veh.* 6(2), 2013, https://doi.org/10.4271/2013-01-2456(2013-01-2456).
35. McAuliffe, B.R. and D'Auteuil, A., "A System for Simulating Road-Representative Atmospheric Turbulence for Ground Vehicles in a Large Wind Tunnel," *SAE Int. J. Passeng. Cars - Mech. Syst.* 9(2), 2016, https://doi.org/10.4271/2016-01-1624.
36. McAuliffe, B.R., Belluz, L., and Belzile, M., "Measurement of the On-Road Turbulence Environment Experienced by Heavy Duty Vehicles," *SAE Int. J. Commer. Veh.* 7(2), 2014, https://doi.org/10.4271/2014-01-2451.
37. Gururaja, P., "Evaluation of Coastdown Analysis Techniques to Determine Aerodynamic Drag of Heavy-Duty Vehicles," SAE Paper 2016-01-8151, 2016, https://doi.org/10.4271/2016-01-8151.
38. Ejsmont, J., Taryma, S., Ronowski, G., and Swieczko-Zurek, B., "Influence of Temperature on the Tyre Rolling Resistance," *International Journal of Automotive Technology* 19(1):45-54, 2018.
39. SAE J2452, "Stepwise Coastdown Methodology for Measuring Tire Rolling Resistance," *Surface Vehcile Recommended Practice J2452*, 2008.
40. Waltzer, S., Hawkins, J., Mitcham, A., Lock, A. et al., "Wind Tunnel Evaluation of Potential Aerodynamic Drag Reductions from Trailer Aerodynamic Component Combinations," SAE Paper 2015-01-2884, 2015, https://doi.org/10.4271/2015-01-2884.
41. McAuliffe, B.R. "Improving the Aerodynamic Efficiency of Heavy Duty Vehicles: Wind Tunnel Test Results of Trailer-Based Drag-Reduction Technologies," NRC Report LTRAL-2015-0272, National Research Council Canada, 2015.
42. Anderson, J., *Fundamentals of Aerodynamics* 3rd Edition (McGraw Hill, 2001).
43. McAuliffe, B.R., Sowmianarayanan, B., and Barber, H., "Near-to-Far Wake Characteristics of Road Vehicles Part 2: Influence of Freestream Turbulence and CrossWinds," SAE Paper 2021-01-0949, 2021.
44. McAuliffe, B.R., Sowmianarayanan, B., and Barber, H., "Near-to-Far Wake Characteristics of Road Vehicles Part 1: Influence of Ground Motion and Vehicle Shape," SAE Paper 2021-01-0957, 2021.
45. McAuliffe, B.R., Sowmianarayanan, B., and Barber, H., "Near-to-Far Wake Characteristics of Road Vehicles Part 3: Influence of Multi-Vehicle Interactions," SAE Paper 2021-01-0959, 2021.
46. Hausberger, S., Rexeis, M., Blassnegger, J., and Silberholz, G. "Evaluation of Fuel Efficiency Improvements in the Heavy-Duty Vehicle (HDV) Sector from Improved Trailer and Tire Designs by Application of a New Test Procedure," Technical Report Report No. I-24/2011 Hb-Em 18/11/679, Institute for Internal Combustion Engines and Thermodynamics, 2011.
47. Ragatz, A. and Thornton, M. "Aerodynamic Drag Reduction Technologies Testing of Heavy-Duty Vocational Vehicles and a Dry Van Trailer," Technical Report NREL/TP-5400-64610, National Renewable Energy Laboratory, 2016.
48. Moomen, M., Rezapour, M., Molan, A.M., and Ksaibati, K., "Assessing Road Load Coefficients of a Semi-Trailer Combination Using a Mechanical Simulation Software with Calibration Corrections," *SAE Int. J. Commer. Veh.* 12(1):31-43, 2019.
49. Duoba, M. and Fernandez Canosa, A. "On-Track Measurement of Road Load Changes in Two Close-Following Vehicles: Methods and Results," in *WCX SAE World Congress Experience*, SAE Paper 2019-01-0755. SAE International, 2019. ISSN 0148-7191. https://doi.org/10.4271/2019-01-0755.
50. Smith, P., Evaluation of Platooning Efficiency for Heavy Duty Trucks using Cooperative Adaptive Cruise Control. Master's Thesis, Auburn University, 2020.
51. SAE J1263, "Road Load Measurements and Dynamometer Simulation Using Coastdown Techniques," *Surface Vehcile Recommended Practice J1263*, 2010.

52. SAE J2263, "Road Load Measurements Using Onboard Anemometery and Coastdown Techniques," *Surface Vehcile Recommended Practice J2263*, 2008.

53. U.S. Environmental Protection Agency and U.S. Department of Transportation, "Greenhouse Gas Emissions Standards and Fuel Efficiency Standards for Medium- and Heavy-Duty Engines and Vehicles," *US Federal Register* 76(179):57106-57513, 2011.

54. McAuliffe, B.R. and Chuang, D., "Track-Based Aerodynamic Testing of a Heavy-Duty Vehicle: Coast-Down Measurements," *SAE Int. J. Commer. Veh.* 9(2), 2016, https://doi.org/10.4271/2016-01-8152.

55. SAE J2978, "Truck and Bus Coastdown Procedure," Surface Vehicle Recommended Practice, work in progress, http://standards.sae.org/wip/j2978/, 2021.

e-ISSN 2641-9645